ANALYSIS OF THE RIGID POROUS MANIFOLD AS AN EFFECTIVE DEVICE TO STRATIFY SOLAR THERMAL STORAGE TANKS

A THESIS
SUBMITTED TO THE FACULTY OF THE GRADUATE SCHOOL OF THE
UNIVERSITY OF MINNESOTA
BY

Vivekananda Ghosh

IN PARTIAL FULFILLMENT OF THE REQUIREMENTS
FOR THE DEGREE OF
MASTER OF SCIENCE

Dr. Jane H. Davidson, Adviser

July 2011

Acknowledgements

I would like to thank my adviser Dr. Jane Davidson for the opportunity to work on this project. This experience has helped me build upon my critical thinking and communication skills and become a better overall engineer. I appreciate all her support and guidance over the past two years.

I would also like to thank Joshua Quinnell for helping me get started with my research as well as always being available to answer questions and offer insight into any problems I came across. I also want to thank him for providing an experimental apparatus to test the stratification manifold and for performing the experiments with me.

I would like to thank Dr. John Carlsson for his assistance in generating an optimization algorithm to use in the manifold simulation.

Finally, I would like to thank my parents and sister for their support and belief in me.

Abstract

One of the most effective and simplest methods to maintain thermal stratification of solar hot water storage tanks during charge and discharge is the use of a rigid porous manifold. The same manifold design can be employed within a novel liquid desiccant solar thermal storage tank to prevent destruction of chemically stored energy during charge and discharge. This type of manifold does not require any moving parts or special materials and thus is particularly appealing for solar thermal storage systems. It has a series of vertical hydraulic resistance elements placed within a perforated tube. At the design operating conditions, the manifold ensures that fluid entering the tank is delivered to the vertical position where it is the same density as the tank fluid. In the present study the utility of a rigid porous manifold is assessed over a range of operating conditions in both a solar hot water and liquid desiccant storage environment.

The primary result is the development of a simple relationship between a dimensionless performance indicator and a second dimensionless parameter that represents the operating condition. A simulation model is used to define this relationship between the operating condition and manifold performance and is applicable to manifolds operating in both hot water and liquid desiccant storage tanks. A plug flow tank model is used to approximate transient tank stratification. Initial modeling suggests off-design operation results in low levels of mixing. Finally, a manifold was built and tested within a prototype liquid desiccant tank. Results show that the design returns low density fluid through the bottom of the tank at a significantly reduced mixing rate compared to free discharge. The same manifold design is able to return high density fluid with minimal mixing.

Contents

List of Tables

List of Figures

Nomenclature

A	Cross sectional area, m^2
D	Manifold tube diameter, m
g	Acceleration of gravity, m/s^2
H	Total tank fluid height, m
h	Density interface height, m
K	Dimensionless pressure loss coefficient, $\frac{\Delta P_o}{\frac{\rho V_m^2}{2}}$
ℓ_d	Spacing between orifice plates, m
M_u	Dimensionless undesired flow rate, $\frac{\dot{m}_u}{\dot{m}_{in}}$
M	Moment of energy, J·m
$\dot{m}$	Mass flow rate, kg/s
MIX	Dimensionless tank stratification, $\frac{(M_{str}-M_{actual})}{(M_{str}-M_{mix})}$
P	Fluid pressure, Pa
P_r	Dimensionless pressure ratio, $\frac{R_o \dot{m}_{in}^2}{\rho_{in}(\rho_t-\rho_{in})g\Delta z}$
R	Flow resistance, $1/m^4$
S	Salt fraction
T	Fluid temperature, K
V	Flow velocity, m^2/s

Greek

ΔP	Change in pressure, Pa
Δz	Change in height, m

ρ	Fluid density, kg/m^3

Subscripts

1	Bottom region
2	Top region
actual	Actual case
c	Initial cold fluid
D	Manifold duct
h	Initial hot fluid
in	Inlet
m	Manifold fluid
mix	Fully mixed case
o	Orifice plate
p	Porous manifold wall
str	Stratified case
t	Tank fluid
u	Undesired flow

Chapter 1 Introduction

1.1 Motivation

1.1.1 Solar Hot Water Tanks

Solar thermal energy has been used extensively for purposes such as domestic hot water and more recently space conditioning. The most common storage medium for solar thermal energy is sensibly heated water. Research has shown that thermal stratification of water storage tanks has a significant impact on overall solar hot water storage system efficiency [1-3]. Thermal stratification refers to a storage state where warm water is stored above cooler more dense water within a single tank. A stratified tank does not exhibit any buoyant plume mixing as the tank fluid is neutrally buoyant. The thermocline is the region of mixing at the interface of the hot and cold fluid regions in the tank. As illustrated in Fig. 1.1(a), the thermocline thickness is zero in an ideally stratified tank. As the fluid in the tank mixes, the thermocline thickness grows (Fig. 1.1(b)). A fully mixed tank is characterized by a uniform temperature distribution (Fig. 1.1(c)).

Thermal stratification offers two main benefits to solar hot water storage system operation [1]. First, maintenance of thermal stratification is necessary to ensure that the usefulness of collected energy is not degraded. After flow passes through the solar collector, the warm return fluid should enter the tank at the vertical location where its temperature equals the temperature of the tank fluid. If the return flow from the solar collector enters below this point of neutral buoyancy, buoyant plume entrainment acts to lower the temperature of the return fluid reducing the quality of the energy to meet the load. Similarly, if return flow from the collector or load enters the tank at a location

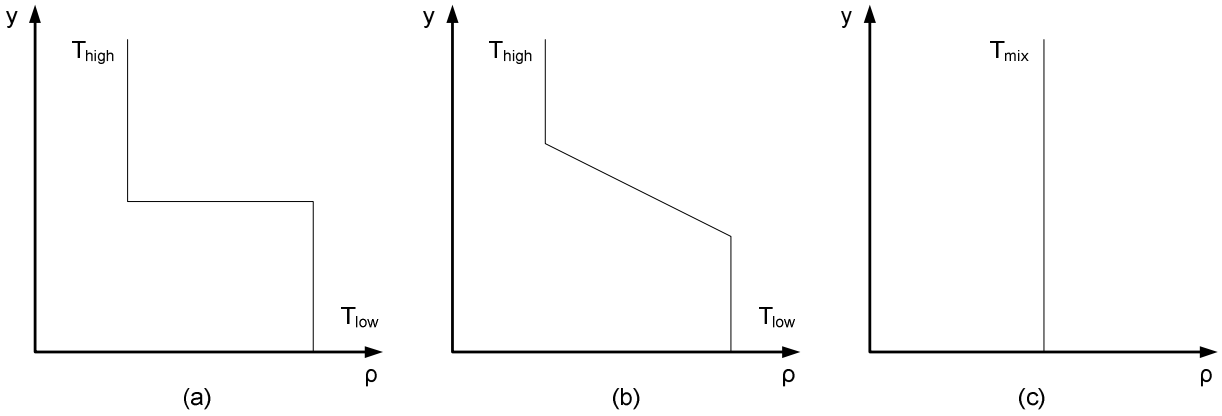

Fig. 1.1: Vertical temperature distributions illustrating various degrees of thermal stratification in a solar water storage tank: (a) Ideal thermal stratification; (b) Partially mixed; (c) Fully mixed

above its point of neutral buoyancy, mixing results in a loss of stored usable energy. Second, thermal stratification increases solar collector performance. If thermal stratification is maintained, the fluid at the bottom of the tank stays cooler for longer during the charging cycle. Both these characteristics help to improve storage efficiencies in solar hot water tanks.

1.1.2 Solar Liquid Desiccant Tanks

A promising new storage medium for solar thermal energy is a liquid calcium chloride solution [4]. Similar to a solar hot water storage system, a liquid desiccant system is capable of storing sensible energy. Additionally, the liquid desiccant medium can store thermochemical storage through desorption of water. Water is desorbed from the liquid desiccant by boiling the solution in a solar collector. Energy is extracted from the concentrated desiccant through reabsorption of water vapor,

$$CaCl_2 \cdot 4.8H_2O(l) + 6.1H_2O(g) \leftrightarrow CaCl_2 \cdot 10.9H_2O(l)$$

$$\Delta h_{326K} = -2560 \ \frac{kJ}{kg_{H_2O}} \tag{1.1}$$

Concentrated liquid desiccant exhibits a higher salt mass fraction, where salt mass fraction is defined as

$$S = \frac{M_{salt}}{M_{solution}} \tag{1.2}$$

The average enthalpy of dilution can be evaluated from the initial and final salt mass fraction of the liquid desiccant solution as shown in eq. (1.1).

$$\bar{h}_d = \frac{1}{\Delta S}\int_{S_{min}}^{S_{max}} h_d \, dS \tag{1.3}$$

The total energy density of the tank over a seasonal cycle is a function of thermochemical and sensible storage. Thermochemical energy is an attractive long-term storage concept as it has no associated thermal losses. Calcium chloride has shown to be a promising desiccant material as it is relatively inexpensive, non-toxic, and environmentally safe.

To increase storage density and reduce system cost, the use of a single tank to store both diluted and concentrated desiccant solutions is under investigation [4]. However, any mixing of concentrated and diluted solution within the storage results in a release of thermochemical energy via reaction (eq. 1.1) and a corresponding increase in sensible energy. The converted sensible energy is not an effective long term storage method as thermal losses will degrade the storage energy density over time. It is therefore important to stratify the tank by density to minimize mixing of concentrated and dilute desiccant. Concentrated liquid desiccant exhibits a higher fluid density and should therefore be stored below dilute desiccant. As with the solar hot water tank, care must be taken to return fluid to its point of neutral buoyancy during charge and discharge cycles. Return fluid entering the tank at an incorrect vertical position results in buoyant plume entrainment and tank mixing.

1.1.3 Stratification Manifolds

An effective and simple method for flow control is a stratification manifold. Stratification manifolds are attached to the tank inlet port and allow flow to exit at the correct vertical location without inducing tank fluid entrainment. Various design strategies have been employed to minimize entrainment of flow into the manifold or outflow below or above the point of neutral buoyancy. A survey of commercial and previously tested manifold designs can be found in Appendix A. Minimization of these undesired flows reduces tank destratification. These same design strategies are applicable to solar thermal liquid desiccant tanks as flow into the tank is controlled by the densities of the storage fluid and fluid entering the tank. The rigid porous manifold (RPM) is further examined in the present study as it has been shown to be effective and does not require any moving parts or special materials.

1.1.3.1 Rigid Manifolds

The RPM design, shown in Fig. 1.2, allows for a controlled buoyant inlet jet to seek its point of neutral buoyancy and thus minimizes tank mixing [5]. Incoming fluid is directed through a diffuser to reduce the vertical component of momentum of the inlet fluid. The mean flow velocity is reduced as the flow leaves the diffuser and enters a larger diameter vertical tube. Open area in the tube wall allows for outflow into the tank at any height. As flow rises through the manifold, it passes through a series of identical and equally spaced orifice plates fixed within the tube. These hydraulic resistance elements are sized such that the difference between the manifold and tank fluid pressure distributions, as shown in Fig. 1.3, is minimized until the point of neutral buoyancy. Minimizing the pressure difference across the manifold wall reduces any flow into the

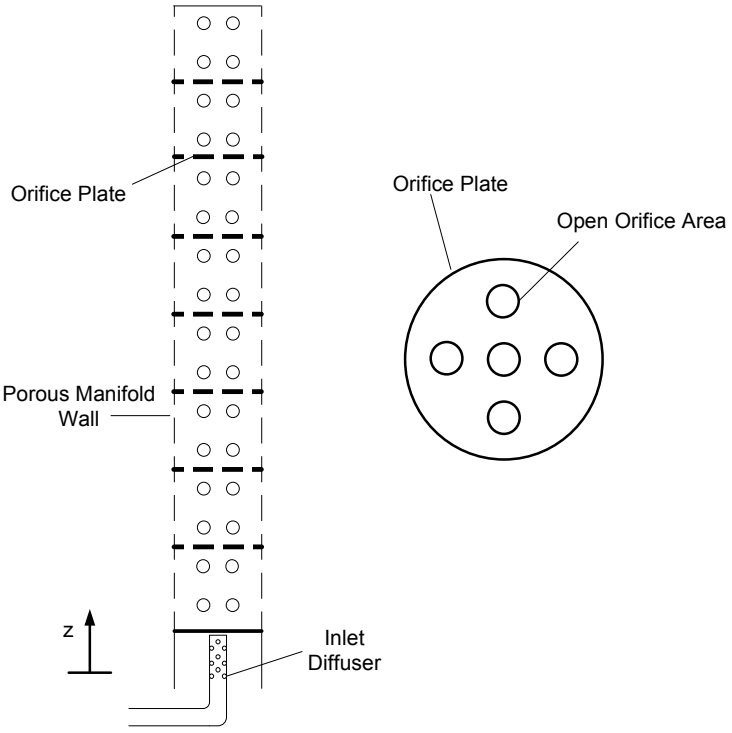

Fig. 1.2: A rigid porous manifold design

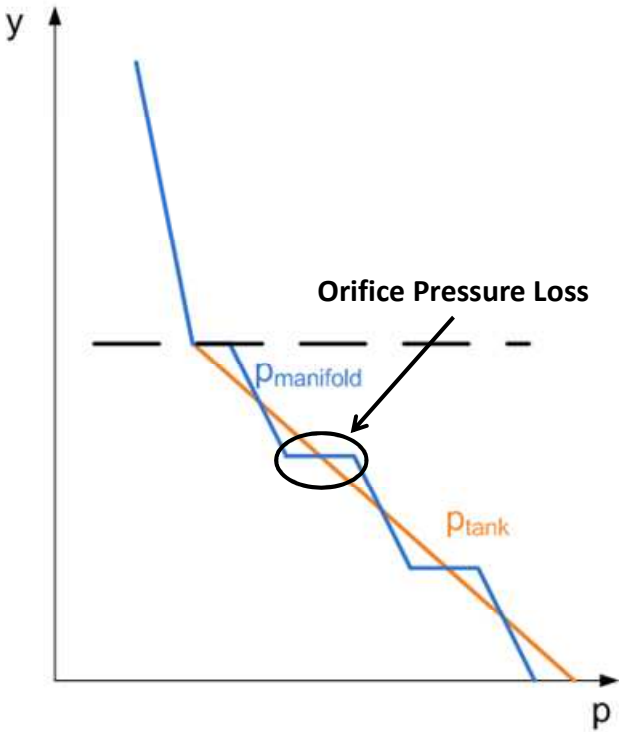

Fig. 1.3: Pressure distribution in tank and manifold fluid

manifold or flow out of the manifold below or above the point of neutral buoyancy. If the manifold is designed properly, fluid entering through the diffuser will flow out of the manifold at the point of neutral buoyancy. Above the point of neutral buoyancy, no flow is passing through the manifold and the tank and manifold pressure distributions are equal.

For flow entering through the bottom of a manifold, the pressure gradient in the manifold fluid can be evaluated from a one-dimensional differential momentum equation [5]

$$\frac{dp}{dy} = -\rho g - \frac{k}{2{A_m}^2}\frac{\dot{m}}{\rho} - \frac{1}{{A_m}^2}\frac{d}{dz}\left(\frac{\dot{m}}{\rho}\right) \tag{1.4}$$

while in the tank the fluid pressure gradient is equal to

$$\frac{dp_t}{dy} = -\rho_t(y)g \tag{1.5}$$

The pressure gradient in the manifold shown in eq. (1.4) is a function of the fluid density, ρ, the orifice loss coefficient per unit length of tube, k, the cross sectional area of the manifold tube, A_m, and the mass flow rate through the manifold, ṁ. Major losses are not considered as they are minimal compared to the minor loss over an orifice plate for the length of tube considered. The orifice loss coefficient, K_o, is defined as the pressure loss across the orifice plate normalized by the upstream dynamic pressure in the manifold.

$$K_o = \frac{\Delta P_o}{\frac{\rho V_m^2}{2}} \tag{1.6}$$

The orifice plates are sized to control vertical manifold fluid pressure distribution such that it is equal to the tank fluid pressure distribution for a given manifold geometry and

operating conditions such as inlet mass flow rate, inlet flow density, and tank density distribution.

Flow through the open area in the manifold wall is a function of the pressure difference across the manifold wall and the associated loss coefficient shown in eq. (1.7).

$$K_p = \frac{\Delta P_p}{\frac{\rho V_p^2}{2}} \tag{1.7}$$

where the pressure drop over the pore wall is normalized by the dynamic pressure of the flow passing through the open area in the wall. As the open area in the manifold wall is increased, flow resistance across the manifold wall is decreased. If the open area is too large, small pressure differences over the manifold wall result in large undesired flow rates at locations where the fluid is not neutrally buoyant. Conversely, as the open area in the manifold wall, flow across the manifold wall is impeded. If flow is not able to fully exit at the point of neutral buoyancy, undesired flow is forced out of the manifold at other heights in the tank [5].

Analytical models have been used to characterize the performance of a rigid porous manifold in a solar hot water storage tank. A one-dimensional system of non-linear differential equations has been used to evaluate the magnitude and location of flows through the porous wall [6]. The results predict that when the open area in the manifold wall is not so small that desired outflow is impeded or so large that undesired flows are amplified, manifold performance is not affected by small changes in open wall resistance. Model results show that orifice plates can be sized to eliminate any undesired flow into and out of the manifold. Undesired flow rates, however, are much more sensitive to small changes in orifice flow resistance. The prior numerical model was

validated through experimentation. The continuous equations were later recast into nodalized equations as a design tool [7], and this approach is used in the present work (see chapter 3.1).

The one drawback of the rigid porous manifold is that the design of the orifice plates is based on a single operating point. The orifice plates are only sized to equilibrate the manifold and tank pressure distributions at a single set of operating conditions. As the operating condition moves away from the design point, undesired flow will increase as a result of the unmatched pressure distributions. Experimental work has shown that the rigid porous manifold is capable of partially stratifying a thermal storage tank at off-design operation [8]. The specific consequences of off-design operation, however, are not well characterized.

1.2 Objectives

In the present study, a dimensionless analysis of the governing equations is provided to develop a relationship between operating conditions and the undesired flow into and out of the manifold. Simulation data define the relationship between the dimensionless parameters. The relationship offers a prediction of undesired flow for a range of operating conditions in a solar hot water tank. Simulation data also quantify the resulting transient tank stratification in a sample hot water storage tank and in a liquid desiccant chemical storage tank. A manifold is constructed for a prototype liquid desiccant tank. Manifold performance is measured through visualization of the flow exiting the manifold as well as measurements of tank fluid salt fraction. The results are used to assess the validity of the design method and the simulation model.

Chapter 2 Theoretical Considerations

At the design operating condition, the rigid porous manifold minimizes the undesired flow through the porous manifold wall. The inlet flow enters the tank at a point of neutral buoyancy and thermal stratification is conserved. At off-design flow conditions, however, undesired flow enters and exits the manifold. The magnitude of the undesired flow is a strong indicator of tank mixing. The location, magnitude, and fluid properties of the flow through the manifold wall at various operating conditions can be calculated using the appropriate fluid flow equations.

The difference between the tank and manifold fluid pressure gradients are minimized from the inlet to the vertical location where the density of the fluid in the manifold equals the density of the storage fluid by selecting the proper vertical hydraulic resistance elements. Given the orientation shown in Fig. 1.2, the vertical pressure gradients in the tank water and manifold flow over the distance between two orifice plates are

$$\nabla P_t = \frac{P_{2t} - P_{1t}}{\Delta y} = -\rho_t g \quad \nabla P_m = \frac{P_{2m} - P_{1m}}{\Delta y} \tag{2.1}$$

where the pressure gradient in the tank is assumed equal to the hydrostatic pressure distribution. Expressions for fluid density of water and calcium chloride are presented in Appendix B. The change in momentum in the manifold flow is minimal, so the manifold pressure gradient expressed in eq. (2.1) reduces to

$$\nabla P_m = -\rho_m \left(g + \frac{K_o \bar{V}^2}{2\ell_d} \right) \tag{2.2}$$

where the orifice loss per unit length, k, is approximated by the loss coefficient over an orifice plate, K_o, divided by the spacing between consecutive orifice plates in the

manifold, ℓ_d. In the present analysis, values of K_o are based on published correlations [10]. The loss coefficient over the orifice plate is a function of the following parameters: the cross-sectional area of the tube, the open area in the orifice plate, the hydraulic diameter of the open area in the orifice plate, the thickness of the orifice plate, and wall friction. Equation (2.2) can be rewritten in terms of a manifold mass flow and orifice resistance,

$$\nabla P_m = -\rho_m \left(g + \frac{R_o \dot{m}_m^2}{\rho_m^2 \ell_d} \right) \tag{2.3}$$

where

$$R_o = \frac{K_o}{2A_m^2} \tag{2.4}$$

The difference in pressure gradients in the tank water and manifold flow is thus,

$$\nabla P_m - \nabla P_t = (\rho_t - \rho_m) g - \frac{R_o \dot{m}_m^2}{\rho_m \ell_d} \tag{2.5}$$

Mass flow into and out of the manifold, $\dot{m}_t$, is driven by unbalanced pressures across the porous manifold wall at vertical locations where the manifold and tank fluid densities differ. The loss coefficient over the open area in the manifold wall (eq. (1.7)) is rearranged to define the net flow rate into the tank at a specific vertical location.

$$\dot{m}_t = \left.\begin{array}{ll} \sqrt{\dfrac{\rho_m [P_m - P_t]}{R_p}} & if\ P_m > P_t \\ -\sqrt{\dfrac{\rho_t [P_t - P_m]}{R_p}} & if\ P_t > P_m \\ 0 & P_t = P_m \end{array}\right\} \tag{2.6}$$

Mass flow into the tank is defined as positive, while flow into the manifold is defined as negative. The pore wall flow resistance is defined as

$$R_p = \frac{K_p}{2A_p^2} \tag{2.7}$$

where A_p is the open pore area in the manifold. The loss coefficient, K_p, is a function of the open area geometry, flow rate through the open area, and velocity of the flow passing through the manifold parallel to the open area. Published correlations for various geometries are available for turbulent flow conditions through the open area. Flow conditions for the operating conditions observed in the rigid porous manifold tend to be in the laminar and transition regime. A trend is provided in the published correlations to approximate the loss coefficient when $Re_p < 10^4$ for various geometries. This trend is based on experiments using an orifice plate design, however, and may be inaccurate in predicting loss coefficients over open area in a tube wall.

The total undesired flow $\dot{m}_u$ is a summation of the net mass flow rate into the tank at vertical locations other than the point of neutral buoyancy.

$$\dot{m}_u = \sum \dot{m}_t \tag{2.8}$$

The undesired mass flow $\dot{m}_u$ is a function of seven parameters including the inlet velocity, the density of the inlet water, the manifold diameter, the difference between the densities in the tank and the manifold, and the vertical distance between the orifice plates.

$$\dot{m}_u = f(g, V_{in}, \rho_{in}, D_m, (\rho_t - \rho_{in}), \Delta P_o, \ell_d) \tag{2.9}$$

The five dimensionless parameters that describe this relationship are

$$\Pi_1 = \frac{\dot{m}_u}{\dot{m}_{in}}, \Pi_2 = \frac{gD}{V_{in}^2}, \Pi_3 = \frac{\Delta P_o}{\frac{\rho_{in} V_{in}^2}{2}}, \Pi_4 = \frac{(\rho_t - \rho_{in})}{\rho_{in}}, \Pi_5 = \frac{\ell_d}{D} \tag{2.10}$$

Π_1 is the undesired mass flow rate normalized by the manifold inlet mass flow rate and can be thought of as a performance parameter. Ideal operation is represented by $\Pi_1 = 0$. The dimensionless parameter Π_2 is the Froude number, which is the ratio of gravitational and inertial forces. Π_3 is the orifice loss coefficient, K_o. Π_4 and Π_5, represent the dimensionless density and a dimensionless length scale, respectively. These dimensionless groups can be combined to produce the relationship

$$\Pi_1 = f\left(\frac{\Pi_3}{\Pi_4\Pi_2\Pi_5}\right) = f\left(\frac{R_o\dot{m}_{in}^2}{\rho_{in}(\rho_t - \rho_{in})g\ell_d}\right) \tag{2.11}$$

In the present study the performance parameter, Π_1, is referred to as M_u and represents the dimensionless total undesired mass flow rate. The dimensionless group on the right hand side of eq. (2.11) is referred to as P_r and is the ratio of the pressure drop across the orifice to the hydrostatic pressure difference between the manifold and tank water. At the design point P_r=1, and ideally M_u=0.

Operation of a rigid porous manifold at $P_r \neq 1$ will result in undesired flows and a reduction in density stratification. For P_r >1, the orifice resistance is too large for the given hydrostatic pressure difference, and fluid will flow from the manifold into the tank at an undesired vertical position where the density of the fluid exiting the manifold is less than the density of the fluid in the tank. The resulting density inversion induces buoyant plume entrainment. In both liquid desiccant and water storage plume entrainment causes a reduction of thermal stratification. Additionally, plume entrainment in a liquid desiccant tank can result in mixing of fluids of different salt fraction. The dilution of the higher salt fraction fluid constitutes a loss in chemical energy storage and an increase in sensible storage. Although no energy is lost from the system in this process, sensible energy is less desirable for energy storage as thermal losses to the environment will lower

the energy density of the tank. For P_r <1, the orifice resistance is too small for the given hydrostatic pressure difference in the manifold and tank, and higher density fluid in the tank will flow into the manifold. For the orientation shown in Fig. 1.2, fluid flow into the manifold will reduce the usable energy content of high temperature fluid. In a liquid desiccant tank, flow into the manifold will also result in a dilution of strong liquid desiccant stored in the tank.

Chapter 3 Methodology

3.1 Governing Equations

We consider charging of a stratified tank. The tank is assumed to be stably stratified into two equal-volumes of ρ_1 and ρ_2 where $\rho_1 > \rho_2$ (Fig. 3.1). Fluid enters the manifold at an intermediate density (ρ_{in}) and mass flow rate ($\dot{m}_{in}$). Ideally, the inlet flow would enter the tank at the interface between the two layers, i.e. at y=h. The manifold must equilibrate the manifold pressure distribution with the pressure distribution in the bottom region of the tank. Therefore, the tank fluid density variable in the definition of P_r is replaced by ρ_1.

$$P_r = \frac{R_o \dot{m}_{in}^2}{\rho_{in}(\rho_1 - \rho_{in}) g \ell_d} \tag{3.1}$$

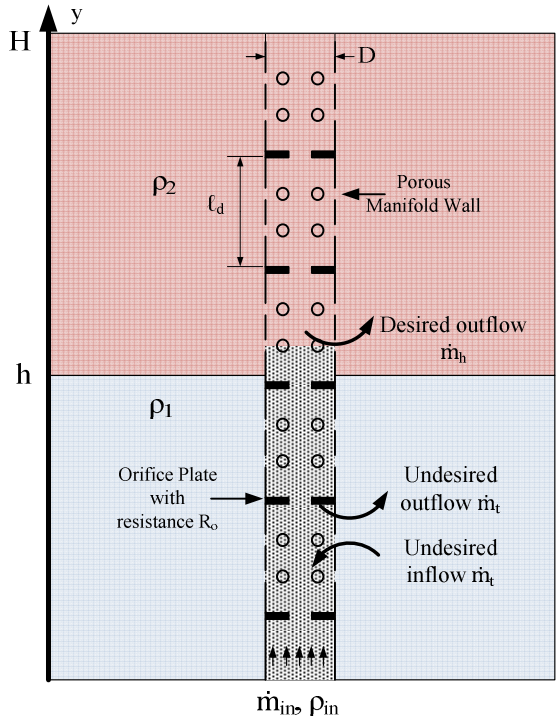

Fig. 3.1: Manifold and tank operating conditions considered in the development of a mixing model for a rigid porous manifold

Nodalized fluid flow equations are numerically solved to determine the flow mass flow rate entering and exiting the manifold [7]. The MATLAB code used to simulate the manifold performance is attached in Appendix C. Figure 3.2 shows the nodal variables needed to describe the manifold performance. The fluid properties in each manifold chamber, or the space confined by two consecutive orifice plates, are represented by a manifold node which is accompanied by a corresponding tank node. Each manifold and tank node is assigned an index, n, starting at the bottom of the tank and increasing in the positive y-direction. At each node, the fluid pressure, temperature, salt fraction, which is equal to zero in the case of a solar hot water storage tank, and mass flow rate through the manifold duct are evaluated. The mass flow rate through the manifold wall is also

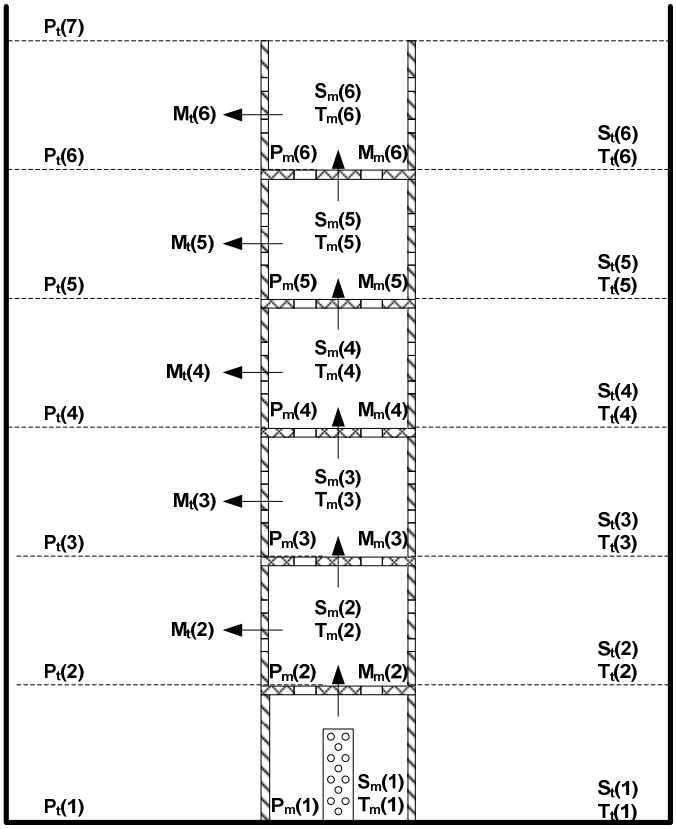

Fig. 3.2: Nodal variables used to describe manifold performance in simulation model

calculated at all manifold nodes except the first node which is the diffuser chamber. At each tank node the salt fraction, temperature, and pressure are fixed.

A flow chart in Fig. 3.3 shows the solution procedure for evaluating the manifold performance. The initial tank fluid temperature and salt fraction distributions as well as the flow rate, temperature, and salt fraction of the flow entering the manifold through the diffuser are defined by the user. An initial range of guess values for the pressure at the bottom of the manifold, $P_m(1)=[P_{low}\text{-}P_{high}]$, must also be provided. The pressure of the tank fluid at each node is calculated using the specified salt and temperature distributions and assuming hydrostatic conditions. Equation (2.1) can be modified to define the pressure difference between consecutive tank nodes.

$$P_t(n) - P_t(n+1) = \rho_t(n) g \ell_d \tag{3.2}$$

The initial guess for the pressure at the bottom of the manifold is evaluated by taking the average of the minimum and maximum values of the provided range. The pressure of the fluid at the next downstream node can then be evaluated using a modified form of eq. (2.3)

$$P_m(n) - P_m(n+1) = \rho_m(n) g \ell_d + \left(\frac{R_o \dot{m}_m(n)^2}{\rho_m(n)} \right) \tag{3.3}$$

The mass flow through the porous wall at each node is given by

$$\dot{m}_t(n) = \left\{ \begin{array}{ll} \sqrt{\dfrac{\rho_m(n)[P_m(n) - P_t(n)]}{R_p}} & if\ P_m > P_t \\ -\sqrt{\dfrac{\rho_t(n)[P_t(n) - P_m(n)]}{R_p}} & if\ P_t > P_m \\ 0 & P_t = P_m \end{array} \right\} \tag{3.4}$$

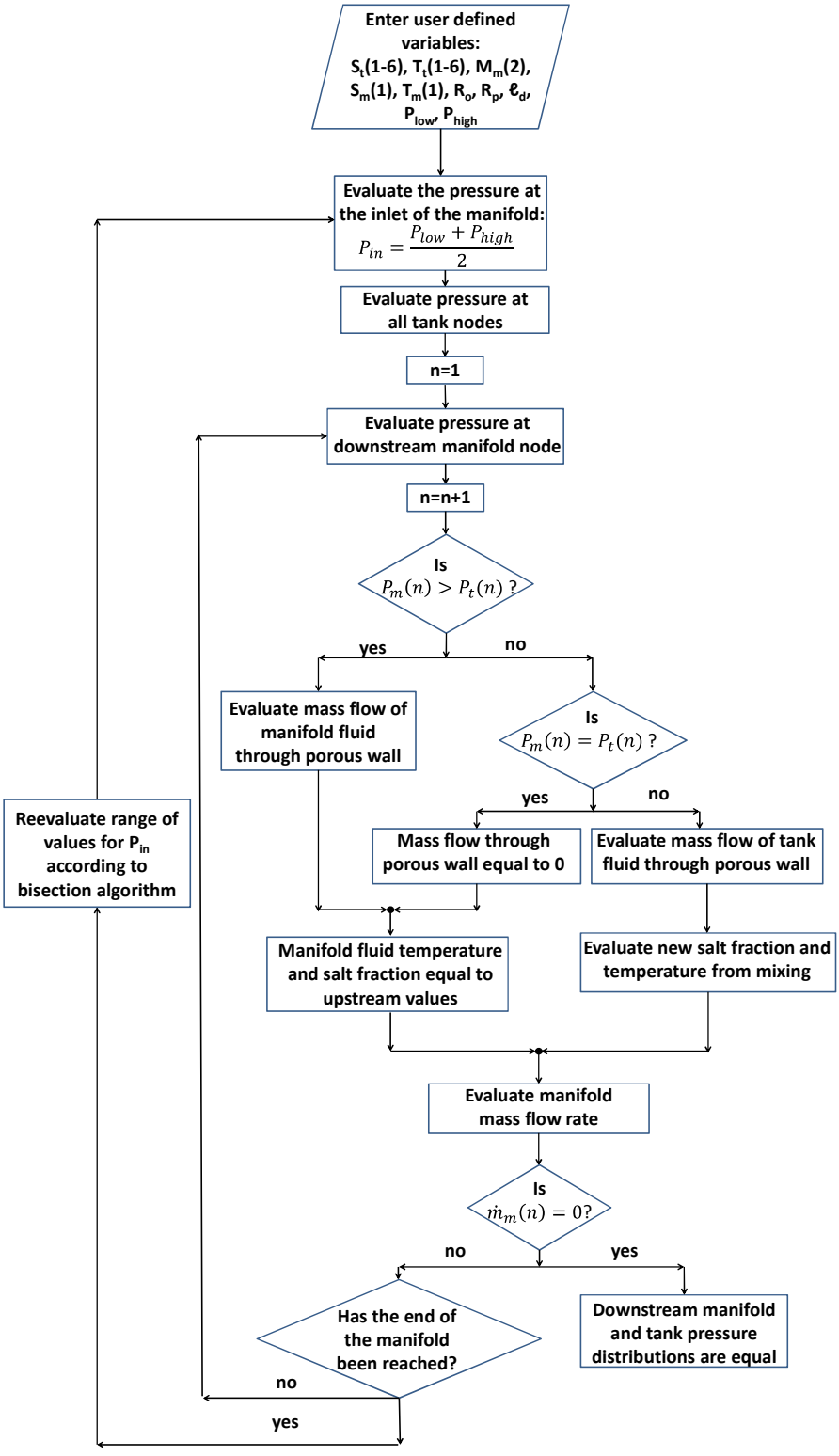

Fig. 3.3: Flow chart visualizing manifold performance code solution procedure

If flow is exiting the manifold at a node or the flow rate through the manifold wall is equal to zero, the fluid temperature and salt fraction are unchanged from the upstream node. For a negative mass flow, or flow into the manifold through the porous wall, fluid temperature and salt fraction must be reevaluated to account for mixing. The mixed temperature is calculated as

$$T(n+1) = \frac{\dot{m}(n)c_p T(n) - \dot{m}_t(n)c_{p,t}T_t(n)}{\big(\dot{m}(n) - \dot{m}_t(n)\big)c_p} \tag{3.5}$$

The temperature of the tank fluid, T_t, depends on whether the node is in the bottom or top half of the tank. The specific heat capacity of water is a weak function of temperature. For a liquid desiccant, however, the specific heat capacity depends strongly on the salt mass fraction. In a liquid desiccant storage tank, the new manifold salt fraction can be evaluated using a salt mass conservation equation,

$$S(n+1) = \frac{\dot{m}(n)\cdot S(n) - \dot{m}_t(n)\cdot S_t}{\dot{m}(n+1)} \tag{3.6}$$

The mass flow rate at the downstream manifold node is a summation of the flow rate at the previous node and the flow through the manifold wall.

$$\dot{m}(n+1) = \dot{m}(n) - \dot{m}_t(n) \tag{3.7}$$

If the mass flow rate evaluated from eq. (3.7) equals 0, then all the flow entering the manifold has exited the manifold through the porous wall and mass continuity within the manifold has been achieved. No flow enters the downstream manifold chambers and the fluid properties at all subsequent manifold nodes are equal to the corresponding tank node. If the mass flow rate evaluated from eq. (3.7) is greater than zero and there are more chambers downstream of the current node, the process is repeated and eqs. (3.3-3.7) are solved to find the fluid properties at the downstream node. If the end of the manifold

is reached or eq. (3.7) results in a negative mass flow rate, a new pressure at the bottom of the manifold must be guessed and the simulation procedure must be repeated. The pressure is guessed through a bisection algorithm. If flow reaches the end of the manifold and a net mass balance of the flows through the manifold is not equal to zero, the pressure at the bottom of the manifold is lower than the true value. This guess value of the pressure at the bottom of the manifold is then assigned as the new lower limit of the range of values used to guess the pressure. Conversely, if eq. (3.7) ever results in a negative mass flow rate, the guess value of pressure at the bottom of the manifold is too high, and the new upper limit of the range of pressure values is updated to this guess value. A new guess value is evaluated by taking the average of the lower and upper limits of the corrected pressure range and the process is repeated until the correct value is found.

The total undesired mass flow is calculated as the sum of the mass flow through the porous manifold wall at all nodes except the two adjacent to the position where the charge fluid should enter the tank. For the assumed conditions shown in Fig. 3.2, the total undesired mass flow equals.

$$\dot{m}_u = \dot{m}_1 + \dot{m}_4 + \dot{m}_5 \tag{3.8}$$

To characterize manifold performance at off-design operation, the numerical model is used to evaluate the undesired mass flow rate at varying operating conditions. These results define a relationship between a dimensionless operating condition and the instantaneous undesired mass flow rate.

3.2 Tank Mixing Model

The degree of mixing within the storage fluid as a result of manifold operation can only be fully quantified through experimentation or a 3-D computational fluid dynamic model that couples fluid flow with heat transfer. In this study a simplified plug flow tank model is used to estimate the impact of operating a manifold at off-design conditions. The plug flow model assumes that tank fluid properties are a function of vertical position [11]. Flow enters or exits the tank through addition or subtraction of discrete volumes of constant property fluid from the tank profile at fixed locations. If a volume of fluid is added to a tank such that a density inversion is created, it is assumed that buoyant flow results in mixing. The inverted layers are mixed to form one layer of constant fluid properties. To conserve the mass of fluid within the tank, a volume of fluid equivalent to the volume added through the manifold is removed from the tank.

Discrete time steps are used to evaluate transient tank stratification as a function of manifold operation. The instantaneous tank mass flows and density distribution are assumed to be constant over a single time step. Integration of the mass flows leads to volume elements that can be added or subtracted from the tank profile at the corresponding chamber height. Energy and mass balances are used to evaluate the new tank fluid properties resulting from density inversions. The mixed temperature is evaluated from a sensible energy balance

$$T_{new} = \frac{m_1 c_{p,1} T_1 + m_2 c_{p,2} T_2}{(m_1 + m_2) c_{p,new}} \tag{3.9}$$

where the specific heat capacities are assumed constant in solar hot water storage. In a liquid desiccant tank, the new salt fraction is evaluated as,

$$S_{new} = \frac{m_1 S_1 + m_2 S_2}{m_1 + m_2} \tag{3.10}$$

As two layers of different salt fraction mix, the fluid volume of initial high salt fraction (S_{max}) will absorb a mass of water (m_w) desorbed by second layer to reach the new mixed salt fraction (S_{new}). This absorption process results in a release of energy. Desorption of water in the second layer is an endothermic process. The net energy release of the layer mixing is calculated as follows [4],

$$E_{hd} = m_w \frac{1}{\Delta S} \int_{S_{new}}^{S_{max}} h_d \, dS - m_w \frac{1}{\Delta S} \int_{S_{min}}^{S_{new}} h_d \, dS \tag{3.11}$$

The shape of the differential heat of dilution curve is such that the mixing process always results in a net release of energy. The absorption energy is converted to sensible energy in the fluid layer, providing an additional temperature rise.

The resulting thermal stratification is quantified by the MIX number [12]. The MIX number defines a height weighted moment of energy to quantify the thermal stratification in a storage tank.

$$M_E = \int_0^H y dE = \sum_i y_i E_i \tag{3.12}$$

The integral formulation of the moment of energy can be converted into a summation by breaking the tank into different nodes, i. The height, y, is measured from the bottom of the tank. For the hot water storage tanks considered, E is defined as the thermal energy of each node. The MIX number is reported by normalizing the experimental or simulation moment of energy with a perfectly stratified and fully mixed moment of energy.

$$MIX = \frac{(M_{str} - M_{actual})}{(M_{str} - M_{mix})} \tag{3.13}$$

A MIX number closer to 0 denotes a temperature stratification profile closer to a fully stratified tank, indicating strong stratification performance.

3.3 Simulation Test Case

To assess manifold performance in a solar hot water tank, a 366 liter storage tank with a height of 1.2 m and cross sectional area of 0.305 m^2 is considered. The manifold is designed for $\dot{m}_{in}$ = 0.07 kg/s and T_{in} = 308 K for a tank with two fluid regions of equal volume at temperatures of T_1 = 293 K and T_2 = 323 K. The manifold tube is modeled with an inner diameter of 7.62 cm (3 in.). Two manifold designs are analyzed: an eight chamber manifold with orifice plates spaced 0.15 m apart and a six chamber manifold with orifice plates spaced 0.2 m apart. The orifice plates in the six and eight chamber manifold are sized to resistances of 1.653 x 10^6 $1/m^4$ and 1.240 x 10^6 $1/m^4$ respectively. These resistances correspond to open orifice areas of 804 mm^2 and 907 mm^2. To evaluate off-design operation, the operating conditions are varied as follows: 0.05 kg/s $\leq \dot{m}_{in} \leq$ 0.09 kg/s, 303 K $\leq T_{in} \leq$ 313 K, and an initial tank temperature distribution, 288 K $\leq T_1 \leq$ 298 K. For these conditions, 0.51 $\leq P_r \leq$ 1.65. For the flow conditions considered, simulation data show that wall resistance values of 1.5 x 10^5 $1/m^4$ to 1 x 10^6 $1/m^4$ have a negligible effect on manifold performance. The open pore area in the tube wall is designed to 2000 mm^2, corresponding to a resistance of 2.5 x 10^5 $1/m^4$. As long as $T_2 > T_{in}$, a change in T_2 does not affect manifold performance. To correlate the dimensionless performance parameter M_u with the dimensionless operating condition, P_r, a numerical simulation is used to evaluate undesired flow at each operating condition.

A similar charging case is modeled for liquid desiccant storage. An initially stratified tank is considered with two equal volume layers of fluid where $S_1 > S_2$. The tank fluid and return fluid are isothermal. Fluid is returned to the tank at an intermediate salt fraction (S_{in}) and specified mass flow rate ($\dot{m}_{in}$). Tank stratification and latent energy storage are preserved when the inlet flow enters the tank at the interface between the two layers. To numerically model this case a 1200 liter tanks is considered. The base area is designed as 1 m^2 and the tank height is 1.2 m. The manifold is designed for $\dot{m}_{in} = 0.07$ kg/s and $S_{in} = 0.425$. The tank stratification is split into two equal volume layers of salt fraction, S_1=0.50 and S_2=0.35. The manifold is modeled with an inner diameter of 7.62 cm (3 in.) and orifice plates spaced 0.2 m apart. The minimize undesired flow, the orifice plate resistance is sized to 4.72 x 10^7 [1/m^4], corresponding to an open orifice area of 213 mm^2. The open pore area in the tube wall is 2000 mm^2. The following parameter ranges are examined to assess off-design performance: $0.05 \leq \dot{m}_{in} \leq 0.09$, $0.45 \leq S_1 \leq 0.55$, $0.375 \leq S_{in} \leq 0.475$, corresponding to a dimensionless operating condition range of $0.51 \leq P_r \leq 3.012$.

3.4 Experimental Setup

A manifold was constructed to evaluate performance in a prototype liquid desiccant storage tank. The experimental apparatus and method were designed by University of Minnesota Mechanical Engineering PhD candidate Joshua Quinnell [15]. Figure 3.4 shows the experimental facility used to evaluate manifold performance. Experiments are conducted in a 1400 liter glass prototype tank. A draw off tube is used to remove fluid from the tank which is then returned to the top of an immersed heat exchanger. Flow exits through the bottom of the heat exchanger and enters the bottom of a rigid porous manifold. Flow exits into the manifold through openings cut into the wall.

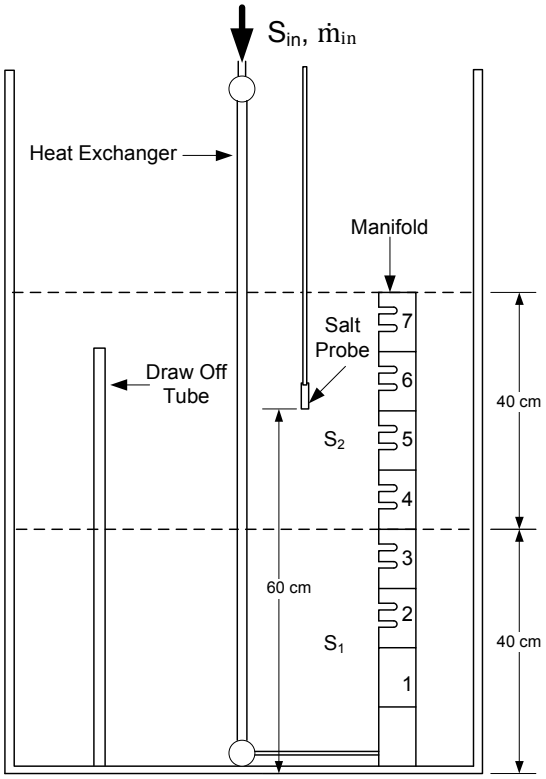

Fig 3.4: Experimental facility

Table 3.1: Design point operating conditions

Inlet Flow Conditions	**Tank Fluid Conditions**
$S_{in} = 0.00$	$S_1 = 0.075$
$T_{in} = 290\ K$	$T_1 = 290\ K$
$\rho_{in} = 998 \frac{kg}{m^3}$	$\rho_1 = 1063 \frac{kg}{m^3}$
$\dot{m}_{in} = 0.07\ \frac{kg}{s}$	

The wall pores are shaped as slots to control the direction of outflow into the tank as well as make flow visualization easier. Flow is visualized through methylene blue dye added

to the fluid entering the draw off tube. The interface between layers of differing salt fraction is measured through a planar laser-induced fluorescence (PLIF) imaging setup. An electrical conductivity probe is also used to measure the change in salt fraction in the top layer of the tank.

The manifold is constructed of ten centimeter long sections of 7.62 cm (3") diameter schedule 40 ABS pipe. The pipe sections are held together through ABS couplings. Orifice plates are cut out of a 0.3175 cm (1/8") sheet of PVC and are cemented into the coupling. The manifold fits into a base attached to the immersed heat exchanger and includes the diffuser. The tank is initially stratified into two equal volume layers of height 40 cm. The layers are isothermal at room temperature of approximately 21°C. The calculations necessary to evaluate the proper manifold design for these operating conditions is shown in Appendix C. The design point operating conditions are shown in Table 3.1. The calculated orifice plate and pore manifold wall resistances are sized to 1.298×10^7 [$1/m^4$] and 2.35×10^5 [$1/m^4$] respectively. The geometry of the orifice plates (Fig 3.5(a)) and chamber sections (Fig. 3.5(b)) are shown. Figures 3.6(a,b) show pictures of the manifold orifice plate and chamber.

Four experiments are conducted to evaluate the performance of the manifold. Experiments 3 and 4 were conducted with a modified pore wall resistance. The experimental operating conditions are shown in Table 3.2.

Table 3.2: Experimental operating conditions

Experiment	R_o [1/m^4]	R_p [1/m^4]	$\dot{m}_{in}$ [kg/s]	S_{in}	S_1	S_2
1	1.298 x 10^7	2.35 x 10^5	0.06	0	0.075	0
2	1.298 x 10^7	2.35 x 10^5	0.035	0	0.075	0
3	1.298 x 10^7	5.36 x 10^6	0.07	0	0.075	0
4	1.298 x 10^7	5.36 x 10^6	0.07	0.075	0.075	0

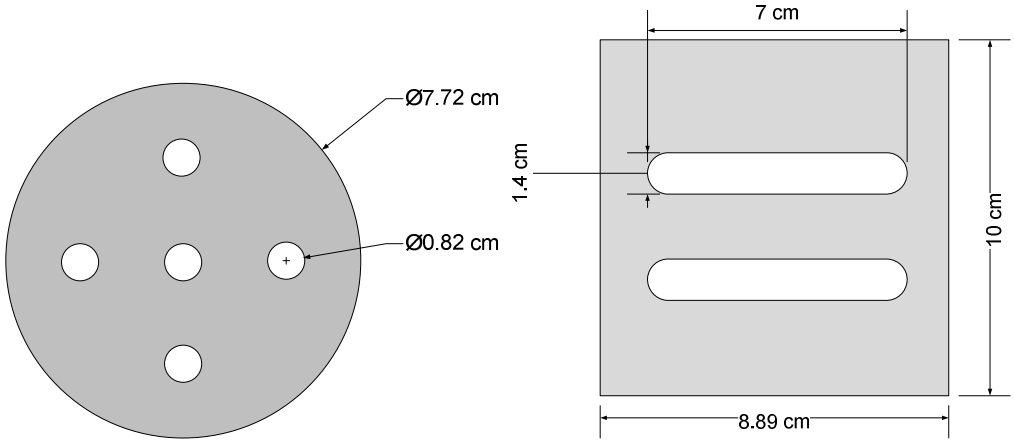

Fig 3.5: Manifold geometry: (a) orifice plate (b) manifold wall

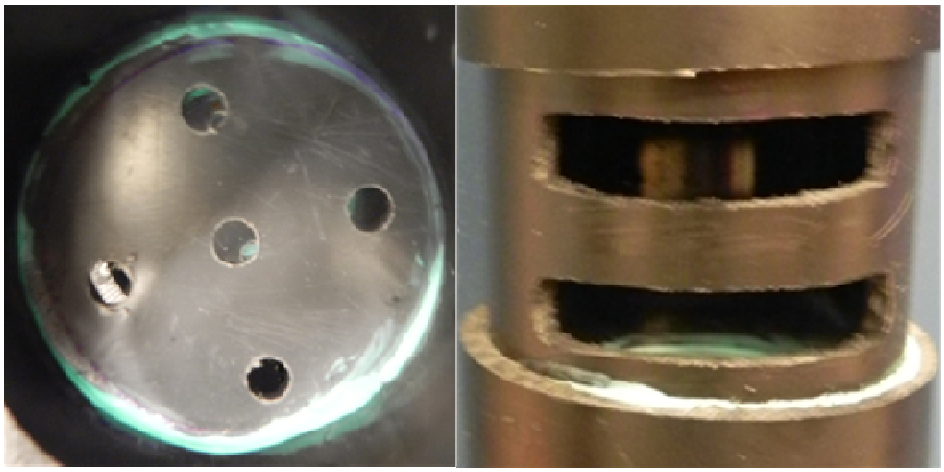

(a) **(b)**

Fig. 3.6: Constructed manifold: (a) orifice plate (b) manifold wall

Chapter 4 Results

4.1. Numerical Model

The primary result is the prediction of the performance index M_u as a function of the dimensionless operating parameter P_r. Figure 4.1 shows this relationship for the manifolds designed for the liquid desiccant and solar hot water storage tanks. The trend shown assumes that wall resistance is within the range of values that does not have a detrimental effect on manifold performance. For the case considered, the results show that a single relationship between P_r and M_u is capable of describing the performance of manifolds operating in both solar hot water and liquid desiccant storage tanks. The total undesired mass flow is a function of the density of the operating fluids rather than the actual salt fraction or temperature of the fluid. The plot provides the designer a tool to interpret the penalty of operating the manifold differently than at the operating conditions for which it was designed. When the operating condition is changed such that the orifice resistance is undersized (P_r <1), flow enters the manifold and mixes with the inlet flow. M_u<0 and becomes increasingly negative as P_r is decreased. Conversely, when the orifice resistance is oversized (P_r >1), flow exits the manifold below the interface at y=h. M_u>0 and increases with increasing P_r. Flow exiting below the interface results in buoyant plume entrainment and a reduction in stratification.

As an example of off-design conditions, consider an increase in the inlet flow rate from the design value of 0.07 to 0.08 kg/s for either case, where P_r =1.31. In this case, the undesired flow rate out of the manifold is 12% of the inlet mass flow rate, or 0.0096 kg/s. Performance is also sensitive to changes in tank and inlet fluid density. P_r is proportional to $\frac{\rho_{in}}{\rho_1-\rho_{in}}$. Therefore, decreasing ρ_1 or increasing ρ_{in} results in P_r <1, whereas increasing ρ_1 or decreasing ρ_{in} results in P_r >1. If the inlet flow temperature for the hot

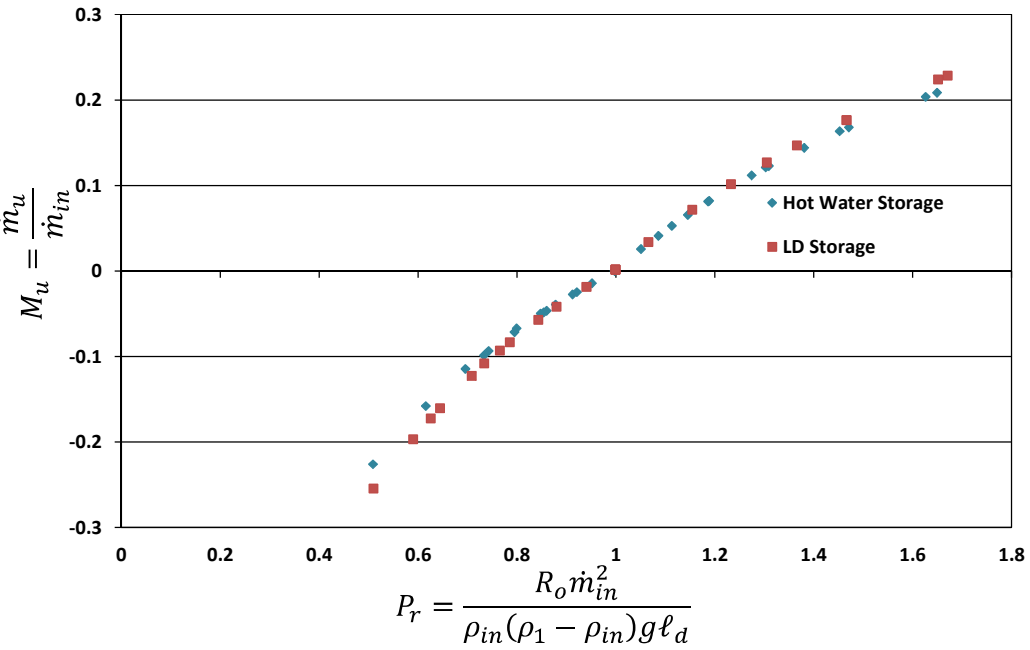

Fig 4.1: Manifold performance in a liquid desiccant and hot water storage tank and different operating conditions

water storage case is increased from the design point at 308 K to 312 K, P_r=0.74. In this case the undesired flow into the manifold is 9 % of the inlet mass flow rate. Manifold performance is more sensitive to changes in ρ_1 and ρ_{in} when the two fluid temperatures are close in value, as $\frac{\rho_{in}}{\rho_1 - \rho_{in}}$ asymptotes at these conditions.

The case of flow entering the manifold at a lower temperature than the fluid at the bottom of the tank, $\rho_{in}<\rho_1<\rho_2$, was also analyzed. In this case, fluid exits the manifold at the lowest chamber regardless of the orifice resistance value. This result indicates the RPM is always an effective method of returning cold, dense fluid to the bottom of the tank. Similarly, prior research has shown the design to be very effective at returning low density fluid ($\rho_{in}>\rho_2>\rho_1$) when the inlet flow is introduced at the top of the tank [6].

To investigate the effect of pore wall resistance on the performance of the manifold, undesired flow is calculated for various pore wall resistances while holding all

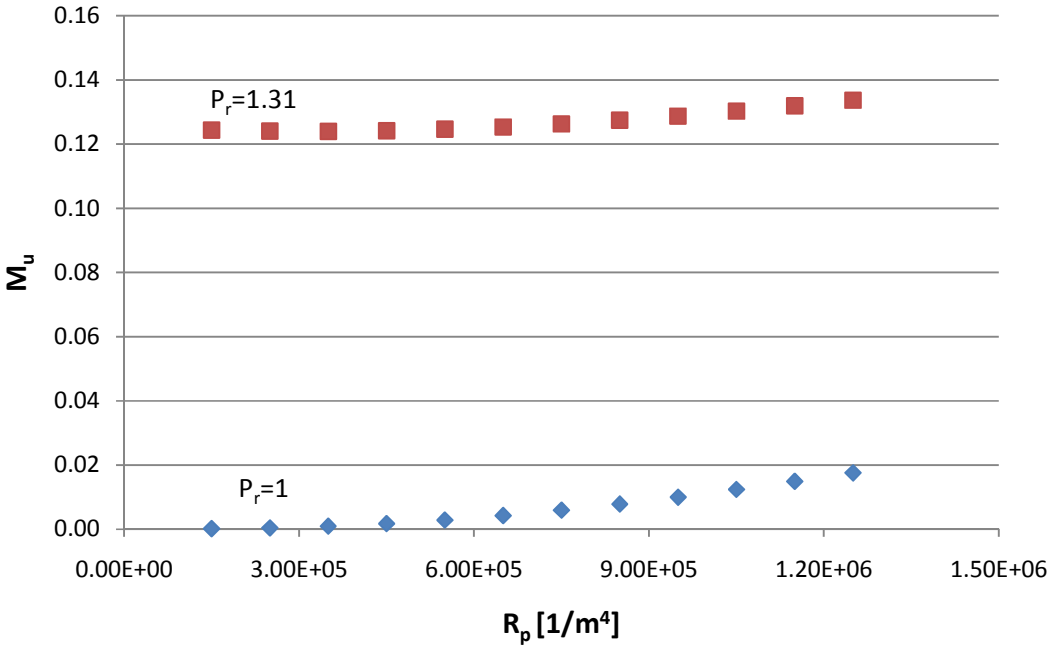

Fig. 4.2: Undesired flow rate as a function of pore wall resistance

other manifold design variables and operating conditions constant. Fig. 4.2 shows simulation results for the hot water storage tank design considered in section 3.3. Two curves are plotted, one at the design point and another at an increased inlet mass flow rate of 0.08 kg/s (P_r=1.31). Wall resistance is varied from 1.5 x 10^5 – 1.25 x 10^6 [1/m^4]. The results show that undesired outflow increases as the wall resistance increases. As the wall resistance increases, outflow at the location of neutral buoyancy becomes more difficult. As a result, some of that flow begins to exit at other vertical locations. Manifold performance, however, is not greatly affected by large wall resistances, as undesired flow does not increase by more than two percent over the range of variables considered. At this time the model is not able to provide results for wall resistances much lower than those considered as the simulation cannot converge to an answer. It is predicted that small pressure gradients across the manifold wall will lead to large amounts of flow when the wall resistance is too low.

The results presented in Figs. 4.1 and 4.2 quantify the extent of undesired flow into and out of the manifold and provide a qualitative measure of the ability of a rigid porous manifold to prevent destratification. Quantification of mixing and the resultant temperature and salt fraction distributions requires a more complete study of the fluid dynamics in the manifold and tank. The most accurate approaches to quantify mixing are extensive experiments and computational fluid dynamic modeling. A simplified approach is presented in this thesis using a plug flow model.

The results from the plug flow tank model for the hot water storage tank are shown in Fig. 4.3; the vertical temperature distribution at the design inlet mass flow rate of 0.07 kg/s (P_r=1) is compared to distributions at 0.05 kg/s (P_r=0.51) and 0.09 (P_r=1.65) when half the tank volume has been cycled. The y-axis represents the dimensionless vertical position in the tank referenced from the bottom of the tank. The difference between the corresponding temperature and initial temperature in the lower half of the tank is shown on the x-axis and is non-dimensionalized by the initial temperature difference in the hot and cold regions of the tank. The plot shows marginal variation in the three temperature distributions above a dimensionless tank height of 0.2. There is very little degradation of the warm fluid in the upper portion of the tank. There is some variation in the thermal stratification in the lower portion of the tank as a result of different mixing patterns. Manifold operation at off-design flow rates of 0.05 kg/s and 0.09 kg/s leads to a more uniform temperature in this region as a result of increased undesired fluid flow from the manifold. Table 4.1 lists the initial values of P_r and M_u when operating at the extremes of the chosen parameter range. These results were obtained by varying one operating parameter while all other variables were held at their

design point values. MIX numbers are very low in all cases. This finding indicates that the rigid porous manifold performs well over a wide rate of operating conditions.

The primary caveat to this interpretation of the results is the inability of the plug flow model to accurately capture the mixing process. The only mixing mechanisms captured by the

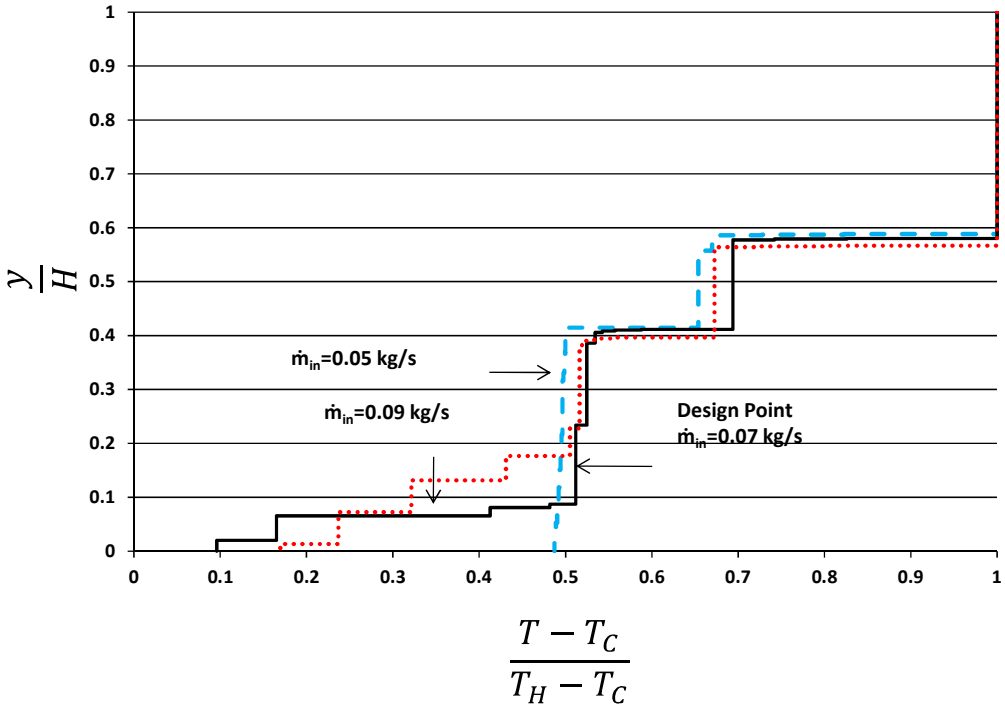

Fig 4.3: Vertical temperature stratification obtained from a plug flow model. Results shown after half the volume has been cycled

Table 4.1: MIX numbers at extremes of parameter range.

	Design Point	Varied Parameter					
		Inlet Temperature [K]		Mass Flow Rate [kg/s]		Tank Temperature [K]	
		303	313	0.05	0.09	288	298
P_r	1	1.63	0.7	0.51	1.65	0.82	1.38
M_u	0	0.2	-0.11	-0.23	0.21	-0.07	0.14
MIX	0.015	0.019	0.033	0.074	0.031	0.017	0.019

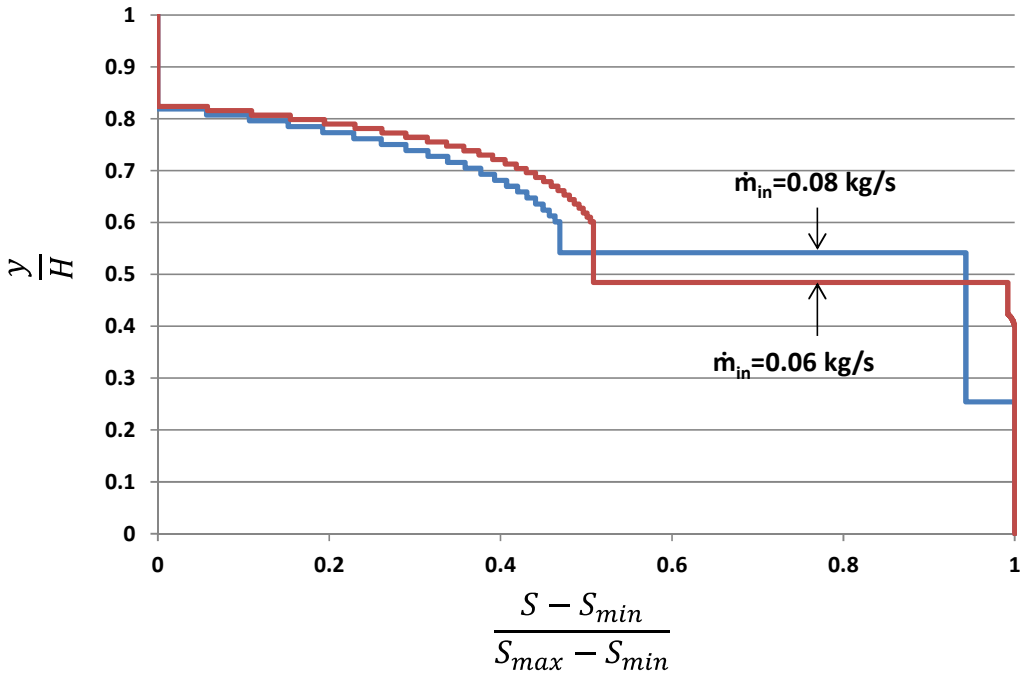

Fig. 4.4: Salt fraction stratification from the plug flow model after 25% of the volume has been cycled

plug flow model are thermal inversions in the tank and mixing of fluid streams within the manifold. It does not capture mixing due to buoyant jet entrainment as flow exits the manifold or suction of tank fluid through the manifold wall. To incorporate these additional mixing mechanisms computational fluid dynamics is required.

Figure 4.4 shows the results of the salt fraction stratification using a plug flow tank model after 25% of the volume has been cycled. Operating both above and below the design flow rate leads to mixing of concentrated liquid with the weaker top layer. Increasing the flow rate to 0.08 kg/s (P_r=1.31) also leads to flow exiting below the interface and release of chemical storage in the tank fluid. Conversely, decreasing the mass flow rate to 0.06 kg/s (P_r=0.734) leads to a larger amount of entrainment of high salt fraction fluid into the weak layer.

4.2 Experimental Results

Experiment 1 was conducted using a PLIF system to track the change in salt fraction concentration within the tank fluid. This transient salt fraction stratification data can be used to track the vertical location of the interface between the liquid desiccant and water layers. Data from the electrical conductivity probe is also used to evaluate the salt fraction of the water layer. At an inlet mass flow rate of 0.06 kg/s, $P_r = 0.73$. At these operating conditions, the numerical model predicts flow to be entrained into the manifold and exit into the water layer. Flow entrainment into the manifold will result in an increase in salt fraction in the water layer as the mixed fluid is expelled from the manifold. During the experiment, however, flow was observed to exit the chambers below the interface, labeled 2 and 3 in Fig. 3.4. Flow predominately exited the top slot in chamber 2. Figure 4.5 shows the PLIF data tracking the interface height over the duration of the experiment. The interface height rose at a fairly constant rate of approximately 0.06 mm/s. The rate of increase seems to imply that the inlet flow is completely exiting into the liquid desiccant layer.

The transient salt fraction data shown in Fig. 4.6 supports this hypothesis, as there is no mixing in the water layer. When the interface reaches the conductivity probe (~600 mm) at around 3000 seconds into the experiment, the measured salt fraction increases rapidly to a constant value of 0.028. All mixing was confined to the volume from the lowest opening in the manifold to the top of the interface height. Liquid desiccant below the lowest opening as well as the water above the interface was undisturbed.

The discrepancy in the predicted and experimental results could be attributed to incorrect sizing of either the orifice plates or wall resistance. If the actual orifice plate

resistance is higher than the calculated value, the modeled P_r value underestimates the actual value and may account for the flow exiting the manifold below the interface. Alternatively, the correlations may overestimate the value of the wall resistance. If the wall resistance is significantly lower than the calculated value, small pressure gradients over the manifold wall would result in the large amount of undesired outflow observed. Experiment 2 tests the hypothesis that the actual orifice resistance is higher than 1.298 x 10^7 [$1/m^4$] and that the wall resistance is properly sized by significantly reducing the inlet mass flow rate ($\dot{m}_{in}$=0.03 kg/s). If the hypothesis holds to be true, the resulting decrease in P_r from the reduced inlet mass flow rate should lead to less undesired flow exiting below the interface. Instead of using the PLIF system to identify the location of the interface, the inlet flow is dyed to identify the exact location of any undesired flow.

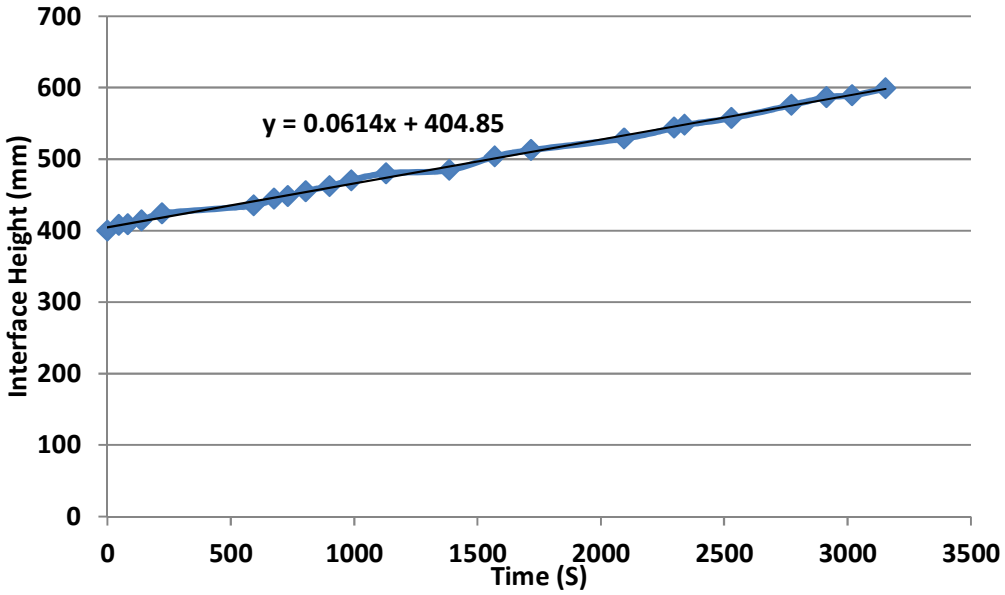

Fig. 4.5: Interface height during the duration of experiment 1.

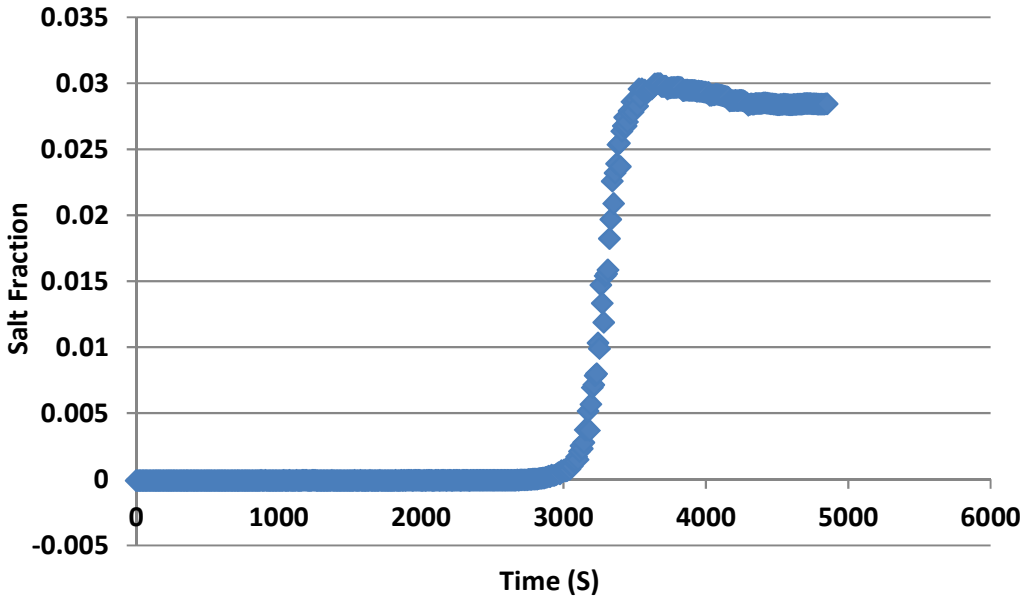

Fig. 4.6: Transient salt fraction data at the conductivity probe location

Flow visualization of experiment 2 showed the same behavior seen in experiment 1. All of the inlet flow exited below the interface, and the water layer was undisturbed. Figure 4.7(a) shows that most of the flow exits the manifold through the top slot in the second chamber. It was much easier for flow to pass through the wall slot than passing through the orifice plate into chamber 2. The water exiting into the salt layer is buoyant and rises after exiting the manifold. The buoyant plume entrains liquid desiccant and the fluid increases in density. The mixed fluid, marked by the dye in Fig. 4.7(b), came to rest below the water layer. The mixed fluid established a density gradient between the water and strong liquid desiccant layers. Fluid below the first opening in chamber 2 remained unmixed.

Reducing the inlet flow rate had no impact on the performance of the manifold. Inlet flow continued to exit below the interface even though the P_r value is presumably well below 1.

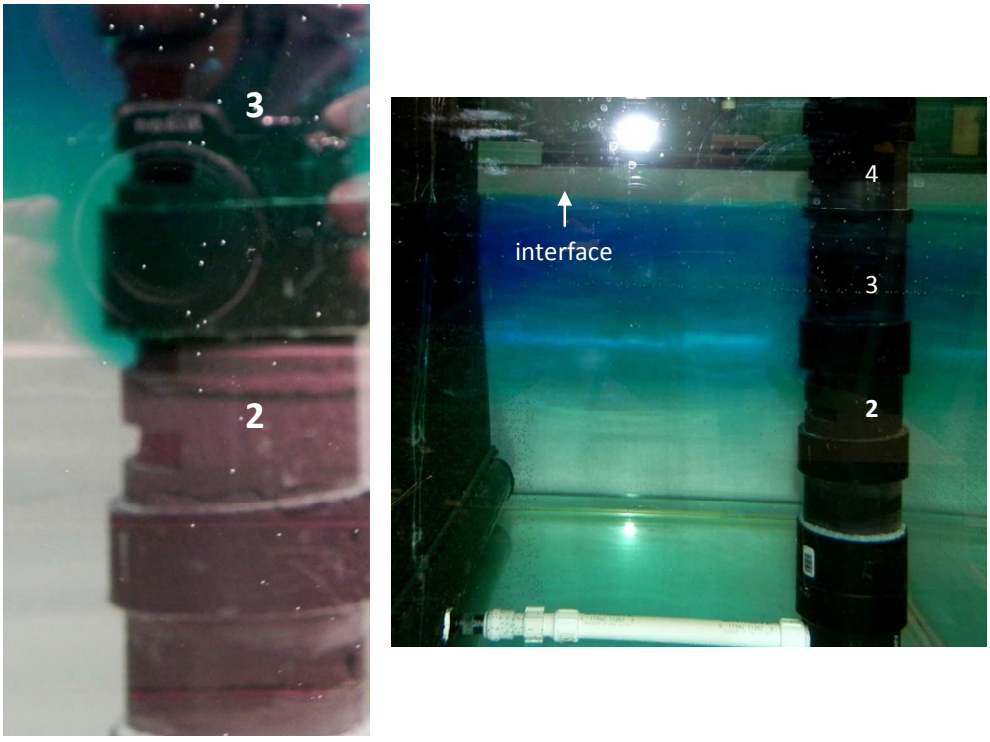

(a) **(b)**

Fig. 4.7: Flow visualization from experiment 2: (a) flow exiting chamber 2 (b) interface location

The results from experiments 1 and 2 indicate that the correlations used were inaccurate in evaluating the open wall resistance. Flow much more readily exited through the pore wall than pass through the orifice plate into the downstream chamber. To increase the pore wall resistance, the open area in the wall was reduced by 75%. The open area in the wall in each chamber is formed by three rectangles of side length 1.4 cm x 1.1 cm, as shown in Fig. 4.8. To test the performance of the new manifold design, experiment 3 was conducted at the design point ($\dot{m}_{in}$=0.07 kg/s) such that any undesired flows into and out of the manifold should be minimized.

A significant improvement was seen in manifold performance as the resistance in the wall was increased. Although some flow was expelled through the bottom two

chambers, the majority of the flow exited into the top water layer. The resulting stratification can be seen in Fig. 4.9. The water layer is now a dark blue while the dye that has been expelled into the salt layer is more dilute. The interface location was visually tracked, and its rate of increase was approximated to be 0.015 mm/s. The rate of

Fig 4.8: Modified pore wall resistance

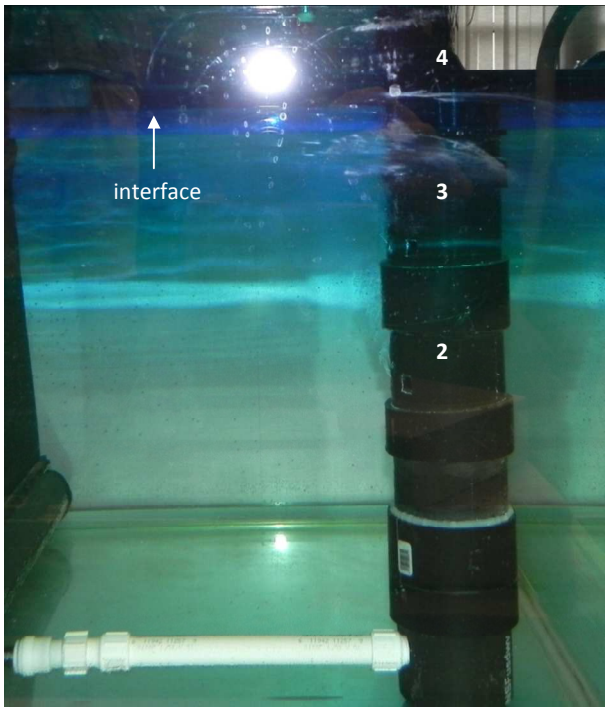

Fig. 4.9: Interface location in experiment 3

increase indicates that 20% of the flow is still exiting below the interface. Flow exiting at chambers 2 and 3 is buoyant and creates a density gradient in between the water and strong liquid desiccant layers.

The undesired flow could be attributed to a larger actual orifice plate resistance compared to the calculated value. A larger actual resistance would correspond to $P_r > 1$ and an increase in undesired flow out of the manifold below the interface. Alternatively, the pore wall resistance may now exceed the range of acceptable values. If the open flow area is too small, outflow above the interface is impeded and flow will begin to exit chambers 2 and 3. To test whether the pore wall resistance is too high to allow for flow, strong liquid desiccant solution is drawn from the tank and fed back into the manifold at the same flow rate as in experiment 3. At this operating condition, flow should exit into the liquid desiccant layer through chambers 2 and 3. Any flow exiting above these two chambers will result in mixing between liquid desiccant and water. If the pore wall resistance is too high, a portion of the flow will leave the manifold above the interface.

Using flow visualization through dye, the manifold was observed to be highly effective at returning dense fluid to the tank. Flow exited into the liquid desiccant layer in horizontal plumes, as shown in Fig. 4.10(a), since the flow was neutrally buoyant. Over the course of the experiment, momentum forces and diffusion mixed the entire liquid desiccant layer as shown in Fig. 4.10(b). Initially, a low flow rate of inlet fluid also exited through the pore wall in chamber 4 above the fluid interface which accounts for the small amount of dyed fluid above the interface. After the first few moments of operation, however, no flow was observed to leave the manifold above the third chamber. After the experiment was completed, the vertical salt fraction distribution was evaluated

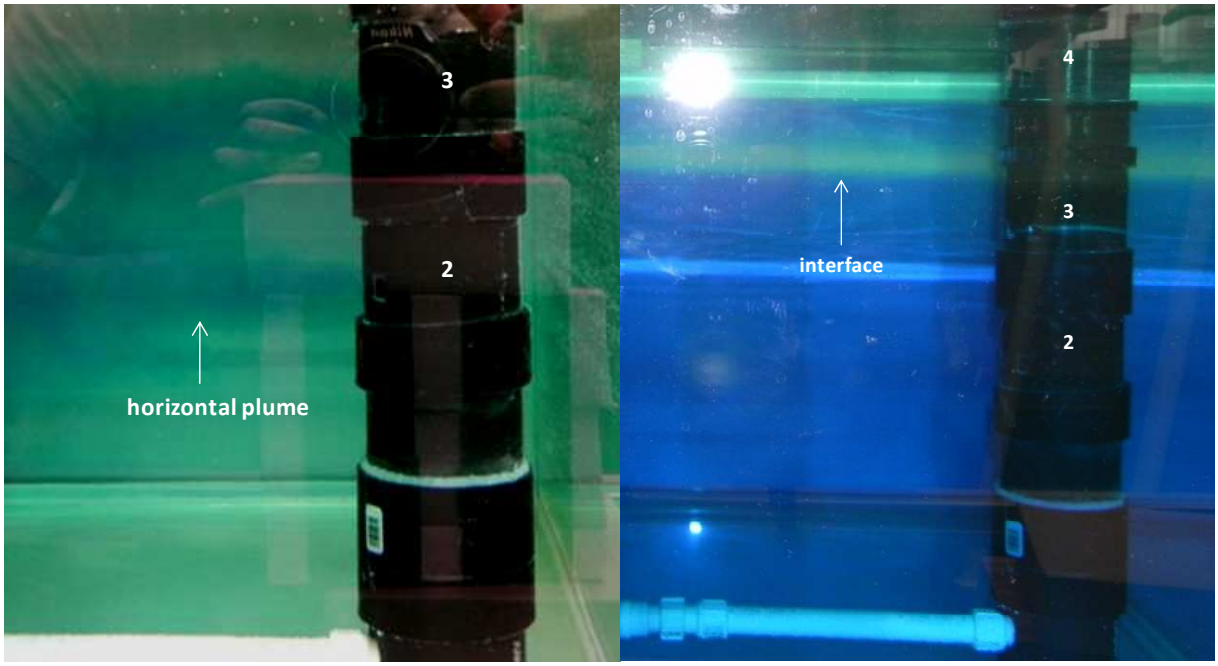

(a) **(b)**

Fig. 4.10: Flow visualization from experiment 4: (a) horizontal plumes exiting manifold into tank (b) final stratification

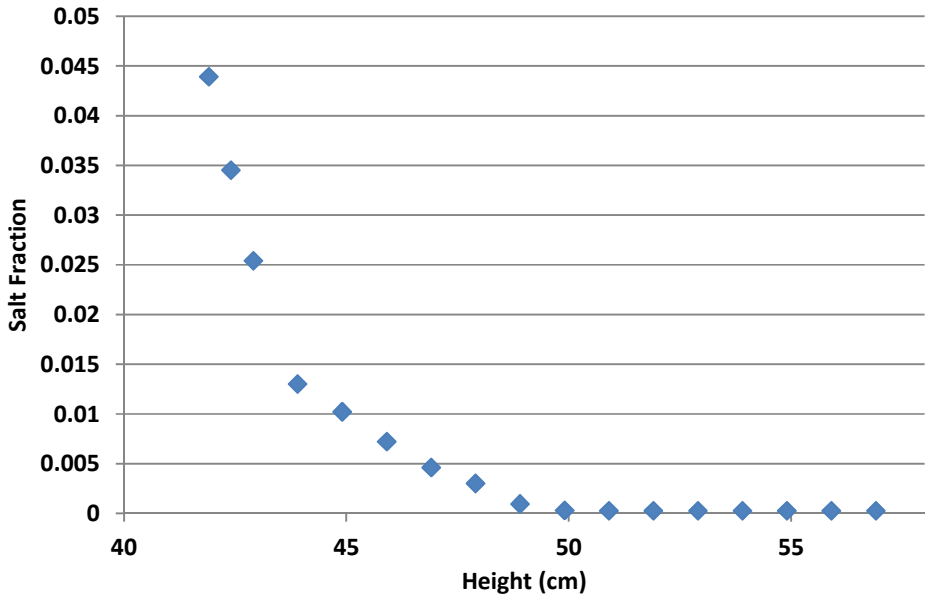

Fig. 4.11: Salt fraction distribution in the water layer from experiment 4

by moving the conductivity probe vertically in the tank. Results in Fig. 4.11 show that salt fraction from the interface (~400 mm) to the original location of the salt probe (~600 mm). The mixing region only extends a few centimeters above the interface. At a height five centimeters above the interface, the salt fraction drops to below 0.01. The plot shows that mixing is minimized within the water layer through the duration of the experiment.

Experiments 3 and 4 indicate that the rigid porous manifold is capable of improving the performance of a liquid desiccant storage system. When cycling fluid through the bottom of the manifold at a low density ($\rho_{in} = \rho_2$), the majority of flow exited into the low density layer. Also, when cycling high density fluid ($\rho_{in} = \rho_1$), mixing above the interface was minimal. Comparing these results to free discharge from the bottom of the heat exchanger, if high density return flow were to be discharged, mixing of the low density tank fluid would be minimized. Returning low density flow, however, would result in large amounts of inlet jet mixing and buoyant plume entrainment. It is obvious from the results of the experiment, however, that the manifold design was not optimized for the chosen operating conditions. The original pore wall geometry used in experiments 1 and 2 was not capable of limiting mass flow through the manifold wall at undesired locations. After the pore wall geometry was adjusted, low density flow continued to exit into the high density layer at a reduced rate in experiment 3. This undesired flow could be a result of improperly sized orifice plates. Manifold performance could be improved through a more accurate prediction of orifice loss and pore wall resistances. Section 5.2 offers some suggestions on more accurate methods to predict these manifold resistances.

Chapter 5 Conclusions and Recommendations for Further Study

5.1 Conclusion

Stratification improves efficiencies of both hot water and liquid desiccant solar thermal storage tanks. A crucial aspect of maintaining stratification is the prevention of fluid mixing in the tank when returning fluid from the load or collector. Arguably, the most effective and simplest method for flow control is an internal stratification manifold. In this study, a rigid porous manifold is analyzed for use in both storage environments. Simulation results show that the effectiveness of the manifold can be expressed by two dimensionless parameters. The first parameter represents the ability of the manifold to prevent undesirable flows into or out of the manifold. The second parameter represents the operating condition relative to the design operating condition. The relationship between these two dimensionless parameters is provided and can be used by the designer to estimate the operating conditions for which a rigid porous manifold will be most effective. At design conditions, the manifold provides nearly ideal conditions. At off design conditions, the manifold is slightly less effective but compared to operation without a manifold still provides significant reduction in mixing.

A rigid porous manifold was constructed to characterize performance in a prototype liquid desiccant tank. The tank was stratified into two water and liquid desiccant layers. The water was circulated through the bottom of the manifold where the desired response was for the flow to pass through the bottom liquid desiccant layer and exit into the water layer. The initial design failed at stratifying the tank as the less dense fluid exited below the interface when operating at low values of P_r. These first couple experiments confirmed that the loss coefficients used to characterize the open area in the

wall were inaccurate. The open area in the manifold wall was reduced by 75% in an attempt to increase the wall resistance. Performance significantly improved with the new redesigned manifold, as the majority of the flow reached the water layer. The experiments conclude that the manifold design reduces mixing when returning buoyant fluid to a storage tank compared to free discharge, and the same manifold design returns high density fluid with minimal mixing.

5.2 Recommendations for Further Study

The results from the experiments indicate that the orifice and pore wall loss coefficients used were not accurate. Instead of applying a correlation, the loss coefficient for the orifice and pore wall geometry used can be evaluated either through computational fluid dynamics or an experimental setup. Experiments can be run at the evaluated design point to obtain best-case results for manifold operation. The simulation code should also be modified to evaluate the lower limit on pore wall resistance that restricts undesired flow exiting the manifold. More accurate approximations for the pore wall loss coefficient can be paired with the modified code to properly design the manifold pore wall.

References

[1] Fanney, A. H. , Klein, S.A., 1988, "Thermal Performance Comparisons for Solar Hot Water Systems Subjected to Various Collector and Heat Exchanger Flow Rates," Solar Energy, 40(1), pp. 1-11.

[2] Lavan, Z, Thompson, J., 1977, “Experimental Study of Thermally Stratified Hot Water Storage Tanks,” Solar Energy, 19(5), pp. 519-524.

[3] Sharp, M. K., Loehrke, R.I., 1979, “Stratified Thermal Storage in Residential Solar Energy Applications,” Journal of Energy, 3(2), pp. 106-113.

[4] Quinnell, J. A., Davidson, J.H., Burch, J., 2011, "Liquid calcium chloride solar storage: concept and analysis," Journal of Solar Energy Engineering, 133, 0110010-1:8

[5] Gari, H. N. and Loehrke, R.I., 1982, "A controlled buoyant jet for enhancing stratification in a liquid storage tank," Journal of Fluids Engineering, 104(4), pp. 475-481.

[6] Gari, H. N. , Loehrke, R.I., and Holzer, J.C., August, 1979, “Performance of an Inlet Manifold for a Stratified Storage Tank,” ASME Paper 79-HT-67, 18th ASME/AIChE Joint National Heat Transfer Conference, 18th, San Diego, Calif., Aug. 6-8, 1979

[7] Davidson, J. H., Carlson, W.T., Duff, W.S., Schaefer, P.J., Beckman, W.A., Klein, S.A., "Comparison of Experimental and Simulated Thermal Ratings of Drain-Back Solar Water Heaters," Journal of Solar Energy Engineering, 115(2), pp. 101-105.

[8] Davidson, J. H., Adams, D.A., 1994, "Fabric Stratification Manifolds for Solar Water Heating," Journal of Solar Energy Engineering, 116(3), pp. 130-136.

[9] Conde, M. R., 2004, "Properties of aqueous solutions of lithium and calcium chlorides: Formulations for use in air conditioning equipment design," International Journal of Thermal Sciences, 43(4), pp. 367-382.

[10]Fried, E. and Idelchik, I.E., 1989, Flow Resistance: A Design Guide for Engineers. New York: Hemisphere Publishing Corporation, pp.87-91.

[11] Duffie, J.A. and Beckman, W.A., 2006, Solar Engineering of Thermal Processes, 3rd edition, Hoboken, NJ: John Wiley & Sons Inc., pp.385-387.

[12] Davidson, J.H., Adams, D.A., and Miller, J.A., 1994, "A Coefficient to Characterize Mixing in Solar Water Storage Tanks," Journal of Solar Energy Engineering, 116(2), pp. 94-99.

[13] Shah, L. J., Andersen, E., Furbo, S., 2005, "Theoretical and Experimental Investigations of Inlet Stratifiers for Solar Storage Tanks." Applied Thermal Engineering, 25(14-15), pp. 2086-2099.

[14] Andersen, E., Furbo, S., 2008, "Investigations on Stratification Devices for Hot Water Heat Stores," International Journal of Energy Research, 32(3), pp. 255-263.

[15] Davidson, J. H, Adams, D.E., 1994, "Fabric Stratification Manifolds for Solar Water Heating." Journal of Solar Energy Engineering, 116(3), pp. 130-136.

[16] Andersen, E., Furbo, S., Fan, J., 2007, "Multilayer Fabric Stratification Pipes for Solar Tanks," Solar Energy, 81(10), pp. 1219-26.

[17] Conde, M., 2004, "Properties of Aqueous Solutions of Lithium and Calcium Chlorides: Formulations for use in Air Conditioning Equipment Design," International Journal of Thermal Sciences, 43(4), pp. 367-382.

Appendix A: Review of Alternate Manifold Designs

Various manifold designs have been proposed and tested for use in solar hot water storage tanks. One such design is manufactured and distributed by Solvis [5]. The design is constructed of PVC pipe which includes only a few large openings into the tank covered by soft hinged flaps. The flaps are seated on the opening such that it is not possible to open into the manifold. Undesired flow into the manifold is therefore minimized. The flaps should open at vertical locations where the pressure inside the manifold exceeds pressure of the tank fluid. A section of this manifold is shown in Fig. A.1. For the conditions and geometry tested, it was found that the stratifier design works best for flow rates between 5 l/min (0.083 kg/s water) and 8 l/min (0.1328 kg/s water). Unfortunately, the flaps do not always work as intended. When the flow rate drops below the optimal range, the passing flow over the wall opening is not large enough to induce a pressure gradient between the tank and manifold and the flap does not close. This malfunction allows fluid from the tank to enter the manifold, which reduces stratification. Low flow rates also lead to a higher rate of heat transfer through the manifold walls. During manifold operation at flow rates above the optimal range, the incoming momentum forces fluid out of all the openings that leads to increased tank mixing. Another source of mixing is the limited amount of openings in the manifold. If the temperature of the incoming fluid matches that of tank fluid in between two opening, the fluid will exit at a non-ideal location, destroying thermal stratification.

Another commercially available design is produced by Sailer [6]. As shown in Fig. A.2, this design is composed of many circular openings that allow for buoyancy driven fluid flow between the manifold and tank. In tests run at ITW in Stuttgart, it was

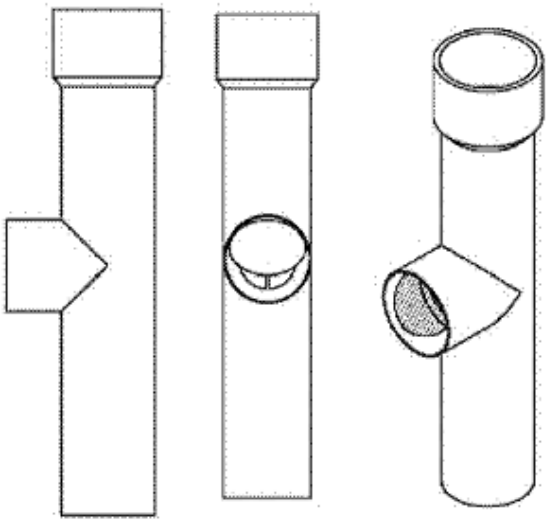

Fig. A.1: Section of the Solvis stratification manifold [5]

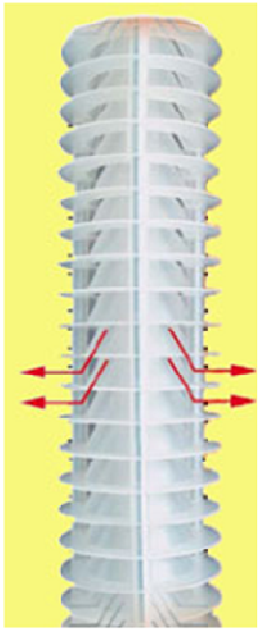

Fig. A.2: Sailer manifold design [6]

found that the manifold was capable of maintaining stratification in an initially stratified tank. Any degradation in stratification at the top of the tank was a result of heat loss from the non-insulated tank. Computational fluid dynamics (CFD) simulations were performed to compare with results from laser induced fluorescence (LIF) measurements.

The simulations offered the benefit of predicting flows in locations that were hard to measure. As expected, the Sailer design showed some undesired inflow as a result of pressure imbalances between the tank and manifold fluids. The magnitude of this mixing was not very large, however. For the operating conditions chosen, the inflow at adverse locations was only 6% of the total flow in the manifold. The CFD simulations also predicted some eddies, which would further promote mixing, at locations where warm manifold water and cold tank water were in contact.

Another type of design is the flexible porous manifold (FPM) [3]. This design consists of a diffuser attached to a fabric sleeve that extends height of the tank. The cross-sectional area of the porous material adjusts itself to control the manifold fluid pressure distribution. When the pressure in the tank exceeds the manifold pressure, the fabric collapses radially to equilibrate the two fluid pressures. This process ensures that no undesired flow enters the manifold at any location. When the pressure in the manifold is slightly larger than that of the tank, the manifold expands radially and fluid exits into the tank through the porous manifold. The FPM is capable of stratifying a tank for variable operating conditions, as the manifold area distribution will adjust as flow rates and temperature vary.

Further research of the porous manifold design includes an investigation on fabric. Synthetic fibers are better suited for use in an FPM as they are not as likely to degrade over time as organic fibers. Also, knit structure, rather than fiber choice, seemed to determine the manifold efficiency. Rib knit fabrics that stretch only in the radial direction perform much better than manifolds constructed of single knit or honeycomb double-knit fabric. When comparing the performance of an FPM constructed of orlon

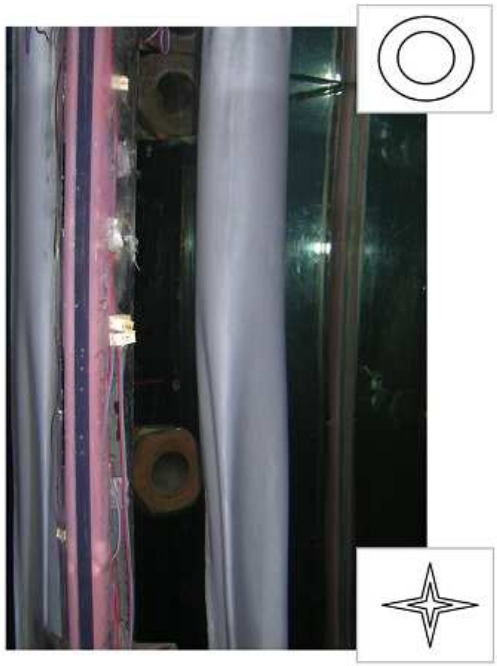

Fig. A.3: A double wall porous fabric manifold showing both expanded and collapsed cross-sections [8]

and a RPM, it was found that the orlon manifold consistently outperformed an RPM operating at off-design conditions in stratifying the tank.

To reduce conductive losses across the fabric, a second fabric layer may be added. For optimal performance the radial separation between the two fabric layers should be close to 10 mm. Different two layer fabric manifold designs, as shown in Fig. A.3, were tested against the Solvis RPM design. It was found that the Solvis design offers better resistance to radial heat transfer to the tank. The two-layer fabric design, however, allows for outflow at any position where the Solvis design is constrained to three discrete outlet locations. These two features offer performance tradeoffs for different operating conditions.

Fig. A.4: Vertical plate stratifier [9]

A unique stratifier design was developed by the International Energy Agency: Solar Heating & Cooling Programme at the Institut für Solartechnik for use in thermal energy storage tanks [9]. The inlet stratifier, shown in Fig. A.4, consists of two parallel plates with a small clearance thickness. On one edge of the plates, the gap is closed while the other is kept open. The inlet flow enters the gap between the plates at a vertical location below the centerline of the tank. As the flow passes through the large surface area of the plates, the flow velocity is significantly reduced. The fluid is then able to seek its point of neutral buoyancy and exit the plates through the open edge. Through flow visualization tests it was found that the inlet flow was able to enter the tank at the correct location while minimizing tank mixing. This manifold concept could be further optimized through various plate spacing or shape adjustments.

Appendix B: Fluid Properties

Fluid properties obtained from experimental curve fit [17].

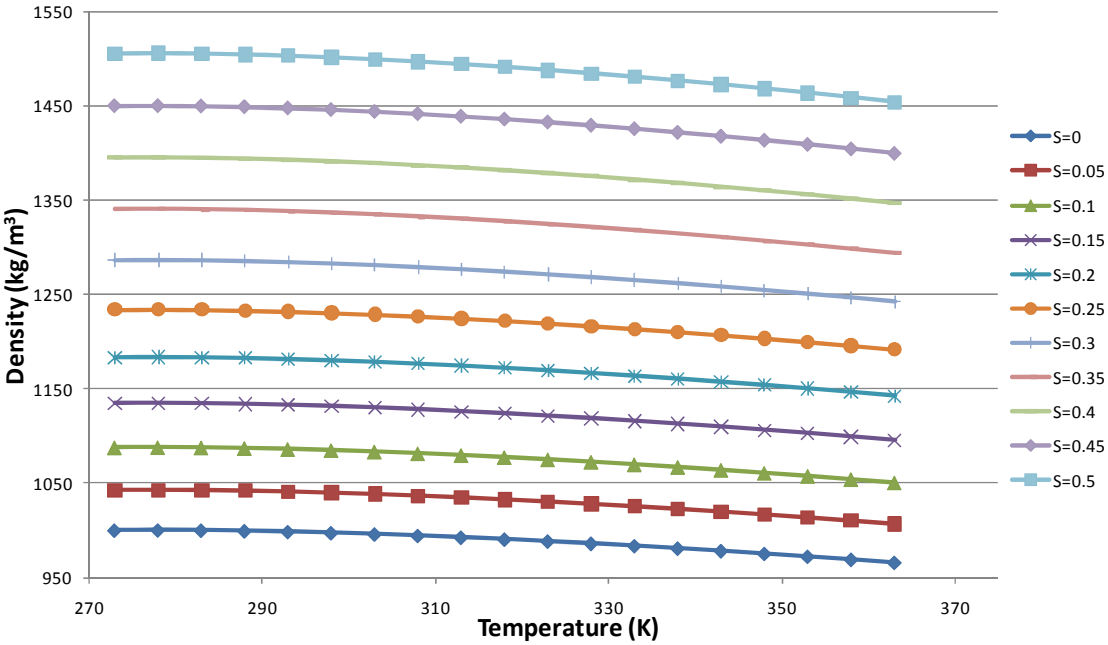

Fig. B.1. Fluid density as a function of temperature and salt fraction

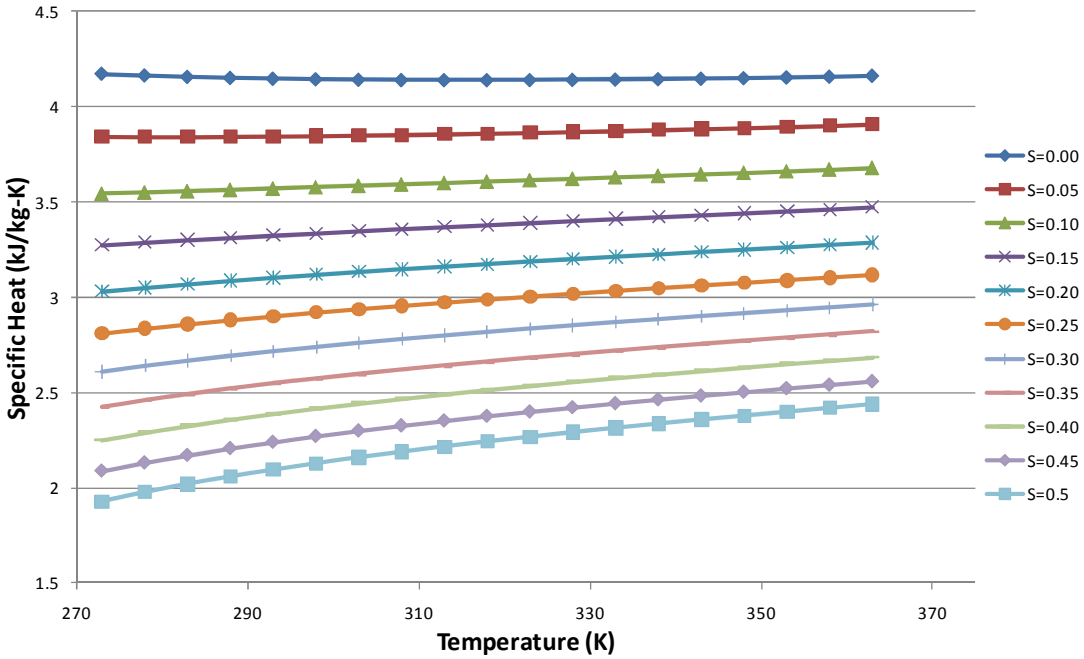

Fig. B.2. Fluid specific heat capacity as a function of temperature and salt fraction

Appendix C: Resistance Sizing

Note: All equations from published correlations use source nomenclature

Orifice Plate

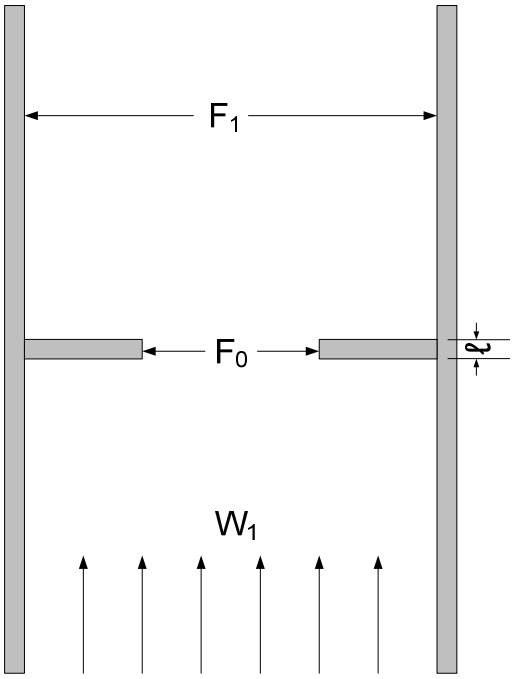

Fig. C.1. Orifice plate geometry and flow conditions

The design point chosen for the experimental conditions is as follows:

$$\dot{m}_{in} = 0.07\ \frac{kg}{s} \qquad \ell_d = 0.10\ m$$

$$S_{in} = 0.00 \qquad S_1 = 0.075$$

$$T_{in} = 290\ K \qquad T_1 = 290\ K$$

$$\rho_{in} = 998\frac{kg}{m^3} \qquad \rho_1 = 1063\frac{kg}{m^3}$$

P_r should equal one at the design point. The equation defining P_r can then be manipulated to evaluate the orifice resistance that minimizes the undesired flow at the design point.

$$R_o = \frac{\rho_{in}(\rho_1 - \rho_{in})g\ell_d}{\dot{m}_{in}^2}$$

$$R_o = \frac{998\ \left[\frac{kg}{m^3}\right]\left(1063\left[\frac{kg}{m^3}\right] - 998\left[\frac{kg}{m^3}\right]\right)9.81\left[\frac{m}{s^2}\right]0.10[m]}{\left(0.07\left[\frac{kg}{s}\right]\right)^2}$$

$$R_o = 1.298 \times 10^7\ \left[\frac{1}{m^4}\right]$$

Using the definition of orifice resistance, the necessary loss coefficient is evaluated as

$$\zeta_1 = 2R_o A_m^2$$

$$\zeta_1 = 2 \cdot 1.298 \times 10^7\left[\frac{1}{m^4}\right](4.681 \times 10^{-3}[m^2])^2 = 568$$

where ζ_1 is the loss coefficient based on the upstream flow velocity, w_1.

$$\zeta_1 = \frac{\Delta p}{\frac{\rho w_1^2}{2}}$$

To evaluate the loss coefficient for an orifice plate when flow is in the laminar or transient regions, Diagram 4-19 (pg. 91) can be used from Fried, 1989

$$\zeta_1 = \zeta_\phi \left(\frac{F_1}{F_0}\right)^2 + \bar{\epsilon}_{0,Re}\zeta_{1quad}$$

where F_0 and F_1 refer to the open area in the orifice plate and upstream respectively, where

$$\zeta_\phi = f\left(Re, \frac{F_o}{F_1}\right)$$

$$\bar{\epsilon}_{0,Re} = f(Re)$$

and ζ_{1quad} is the loss coefficient over the orifice plate at turbulent conditions. The Reynolds number used for these lookups based on the velocity and the hydraulic diameter of the open area in the orifice plate.

$$Re_0 = \frac{w_0 D_h}{\nu}$$

Using the inlet mass flow rate, a function can be written to evaluate the velocity through the orifice plate.

$$w_0 = \frac{\dot{m}}{F_0 \rho}$$

The following curve fit from diagram 4-15 (pg. 87) is used to evaluate ζ_{1quad}.

$$\zeta_{1quad} = \left[\left(0.5 + \tau \sqrt{1 - \frac{F_0}{F_1}} \right) \left(1 - \frac{F_0}{F_1} \right) + \left(1 - \frac{F_0}{F_1} \right)^2 + \frac{\lambda l}{D_h} \right] \left(\frac{F_1}{F_0} \right)^2$$

where l is the thickness of the orifice, and τ is a constant and a function of,

$$\tau = f(l, D_h)$$

The following variables can be calculated immediately.

$$\nu = 1.01 \times 10^{-6} \frac{m^2}{s} \quad F_1 = 4.681 \times 10^{-3} m^2 \quad l = 3.175 \times 10^{-3}\, m$$

All other variables are functions of the open area in the orifice plate. The process is iterative to solve for this value. Using a solver, an open area of 0.0002674 m^2 is needed to obtain a loss coefficient of 568. Five holes are used to obtain the area needed, each of diameter 0.82 cm.

Wall Perforation

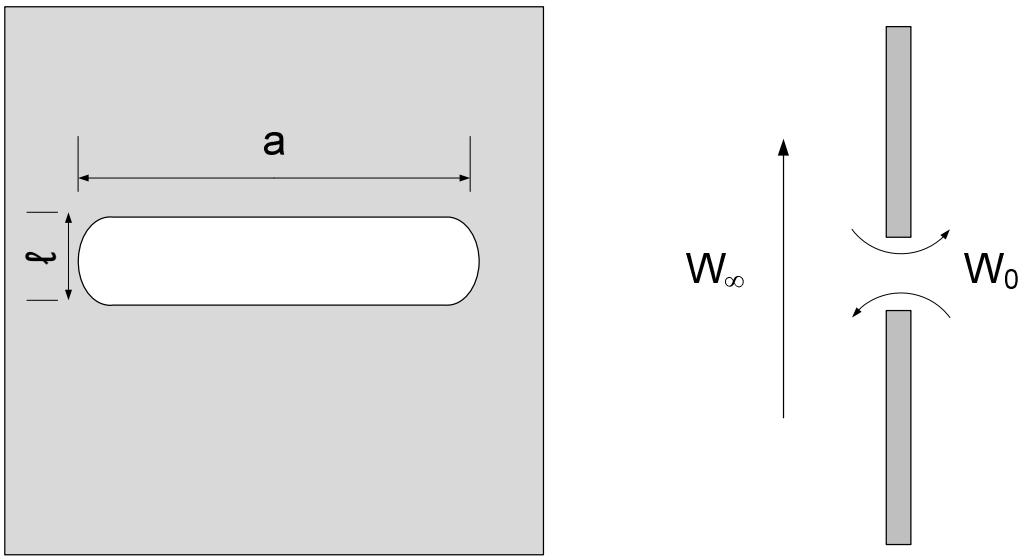

(a) **(b)**

Fig. C.2. Orifice wall geometry: (a) slot in a wall (b) with passing flow

To evaluate the flow resistance of slots in a wall (Fig. C.2(a)) with passing flow (Fig. C.2(b)), correlations presented in Fried and Idelchik are used. Two slots per chamber of width a = 7 cm and height ℓ = 1.4 cm are used to approximate the open area used in previous manifold designs [5, 7]. The loss coefficient for flow through the open area in the wall is defined as follows.

$$\zeta = \frac{\Delta p}{\frac{\rho w_0^2}{2}}$$

For flow conditions where the Reynolds number through the open area equals $Re_0 > 10^4$, the loss coefficient is a function of the following.

$$\zeta = f\left(\frac{w_\infty}{w_0}, \frac{\ell}{a}\right)$$

The wall loss coefficient for all chambers in the manifold is approximated using guess values of w_0. The guess value for velocity through the wall is updated until it converges

with the model solution. For the case of the inlet flow completely exiting through one chamber (ṁ=0.035 kg/s per slot), the loss coefficient is evaluated as

$$\zeta = 2.7$$

The flow conditions in the manifold, however are such that $Re_0<10^4$. No trend data for this exact case at these flow conditions are presented or could be found in alternate literature. The trend in 4-19, which is formulated using data from orifice plate experiments, is used to evaluate an approximate resistance.

The following correlation is used to adjust for the laminar and transient regime.

$$\zeta_1 = \zeta_\phi + \bar{\epsilon}_{0,Re}\zeta_{1quad}$$

$$\zeta_\phi = f\left(Re, \frac{F_o}{F_1}\right)$$

$$\bar{\epsilon}_{0,Re} = f(Re)$$

Where in this case F_0/F_1 is equal to 0. Reynolds number is now evaluated using the velocity and hydraulic diameter of the slot.

$$Re = \frac{w_0 D_h}{\nu}$$

Where w_o represents the velocity through the opening in the wall. The hydraulic diameter of a slot is calculated as

$$D_h = \frac{4A}{P} = \frac{4(1.4 \cdot 7)}{2(1.4 + 7)} = 2.33\ cm$$

The maximum flow rate is 0.035 kg/s per slot, corresponding to a velocity of 0.0353 m/s The Reynolds number is calculated as

$$Re = \frac{998\frac{kg}{m^3}\ (0.035\frac{m}{s})(0.0233\ m)}{1\ \times 10^{-3}\frac{kg}{m \cdot s}} \approx 800$$

At this Reynolds number,

$$\zeta_{\phi} = 0.473$$

$$\bar{\epsilon}_{0,Re} = 0.5$$

$$\zeta_1 = 0.473 + 0.5 \cdot 2.7 = 1.823$$

The resistance is calculated using the total open area of both slots

$$R_p = \frac{1.823}{2 \cdot (.001984\ m^2)^2} = 2.3\ \times 10^5 \frac{1}{m^4}$$

This value falls within the acceptable range of pore wall resistances.

Appendix D: RPM Code

MATLAB code used to solve for the performance of a rigid porous manifold:

```
function [x]=RunRPM
%Starting point in the code that allows for the evaluation of the rigid
%porous manifold equations.  All user defined variables are located here.
%Function currently returns the set of Rp values evaluated and the
%corresponding value for Mu.


n=1;    %counter set

%User defined variables

Ro=4.72e7;   %Define orifice resistance [1/m^2]
Rp=3e5;     %Define wall pore resistance [1/m^2]
T1=290;     %Temperature at bottom half of tank [K]
T2=290;     %Temperature at top half of tank [K}
Tin=290;    %Temperature at manifold inlet
S1=0.5;   %Salt mass fraction at bottom half of tank
S2=0.35;       %Salt mass fraction at top half of tank
Sin=[0.41,0.42,0.425,0.43,0.44,0.45];      %Salt mass fraction at manifold inlet
Min=[0.07];   %Mass flow rate into the manifold
chambers=6; %Number of chambers in the manifold (starting with diffuser chamber)
z=0.2;      %Height of each chamber;

Plow=15000;      %Range of guess values for pressure [pa] at the bottom of the manifold.
Phigh=18000;    %Should be minimized if possible.  Value will be close to pressure at
bottom of tank
while n<=length(Sin)
   %The temperature and salt arrays must be correctly sized for the given
   %number of chambers.

[error,Mu(n),Pr(n)]=Pestimate([Ro,Rp],[T1,T1,T1,T2,T2,T2],[S1,S1,S1,S2,S2,S2],[Plow,
Phigh],Sin(n),Tin,Min,chambers,z);
   n=n+1;
end
 x=[Sin', Mu',Pr']
```

```
function
[error,Mu,Pr]=Bisection(Plow,Phigh,Ro,Rp,Ttank,Stank,Sin,Tin,Min,chambers,z)
%Uses a bisection algorithim over a very small range of pressures to
%the find the pressure at the bottom of the manifold which
%allows for a solution of the manifold performance

%variable intialization
n=1;
y_int=1;


while(abs(y_int)>0.0001) && (n<100)
   %Bisection algorithm-breaks after 100 runs or when error is suitably
   %small
   P_guess=(Phigh+Plow)/2;
   n=n+1;
   y_int=RPMEquations(P_guess,Ro,Rp,0,Ttank,Stank,Sin,Tin,Min,chambers,z);
   if y_int<0
      %If total flow exiting manifold walls is lower than flow entering
      %through inlet, pressure guess is too high.
      Phigh=P_guess;
   else
      %If total flow exiting manifold walls is greater than flow entering
      %through inlet, pressure guess is too low
      Plow=P_guess;
   end
end
n
% P_guess

[error,Mu,Pr]=RPMEquations(P_guess,Ro,Rp,1,Ttank,Stank,Sin,Tin,Min,chambers,z);

end
```

```
function [error,Mu,pi1]=Pestimate(x,Ttank,Stank,P,Sin,Tin,Min,chambers,z)
%Called by RunRPM.m to estimate the pressure at the bottom of the manifold
%which leads to a solution for the manifold equations.  The program uses a
%an intersections algorithm method to approximate the pressure at the bottom
%of the manifold that leads to mass continuity.
%If the pressure guess at the bottom of the
%the manifold is too low, RPMequations.m will return a positive error in
%the mass flow balance.  Conversely, if the pressure guess is too high, a
%negative error is returned.  This knowledge is used to find the pressure
%value that returns the proper result.  Function returns the value of Mu,
%or undesired flow.

Ro=x(1);
Rp=x(2);

error=0;
P=[P(1):1:P(2)];

%Returns an array of values representing the mass flow error for a range of
%pressure values at the bottom of the manifold
 for n=1:length(P)
    [error(n), Mu,
Pr]=RPMEquations(P(n),Ro,Rp,0,Ttank,Stank,Sin,Tin,Min,chambers,z);
 end

c=zeros(length(P),1);

%Finds a rough estimate for the correct P value that gives an error of 0
e=intersections(P,error,P,c);



% Clear necessary values
P=0;
error=0;

% A smaller range is now used to approximate the pressure at the bottom of
% the manifold which results in a mass flow error of 0
Plow=e(1)-5;
Phigh=e(1)+5;

e=0; %clear values


P=[Plow:.001:Phigh];
 for n=1:length(P)
```

```
   [error(n),Mu,Pr]=RPMEquations(P(n),Ro,Rp,0,Ttank,Stank,Sin,Tin,Min,chambers,z);
 end

c=zeros(length(P),1);
%Finds a better estimate for the pressure at the bottom of the manifold
e=intersections(P,error,P,c);
% f2=figure;
% pz=plot(P,int,P,c)



   %FindP gives the actual result for each case
[error,Mu,pi1]=Bisection(e(1)-
.001,e(1)+.001,Ro,Rp,Ttank,Stank,Sin,Tin,Min,chambers,z);


%

end
```

```
function
[error,Mu,Pr]=Bisection(Plow,Phigh,Ro,Rp,Ttank,Stank,Sin,Tin,Min,chambers,z)
%Uses a bisection algorithim over a very small range of pressures to
%the find the pressure at the bottom of the manifold which
%allows for a solution of the manifold performance

%variable intialization
n=1;
y_int=1;


while(abs(y_int)>0.0001) && (n<100)
   %Bisection algorithm-breaks after 100 runs or when error is suitably
   %small
   P_guess=(Phigh+Plow)/2;
   n=n+1;
   y_int=RPMEquations(P_guess,Ro,Rp,0,Ttank,Stank,Sin,Tin,Min,chambers,z);
   if y_int<0
      %If total flow exiting manifold walls is lower than flow entering
      %through inlet, pressure guess is too high.
      Phigh=P_guess;
   else
      %If total flow exiting manifold walls is greater than flow entering
      %through inlet, pressure guess is too low
      Plow=P_guess;
   end
end
n
% P_guess

[error,Mu,Pr]=RPMEquations(P_guess,Ro,Rp,1,Ttank,Stank,Sin,Tin,Min,chambers,z);

end
```

```
function [error, Mu,
Pr]=RPMEquations(P_0,Ro,Rp,print,Ttank,Stank,Sin,Tin,Min,chambers,z)
%Solves the manifold equations given user defined variables, including the
%pressure at the bottom node in the manifold.  Will return the mass flow
%rate error, which is the sum of the flow through the manifold inlet and
%the flow entering or exiting the manifold at all vertical locations.  Mass
%flow rate balance should sum to zero.


%Array initialization

%Pressure in the manifold, with a given pressure at the bottom node
Pm=zeros(1,chambers+1);
Pm(1)=P_0;

%Mass flow rate through the manifold, with a given inlet mass flow rate
Mm=zeros(1,chambers+2);
Mm(2)=Min;

%Mass flow rate through the manifold wall
Mt=zeros(1,chambers+1);

%Salt mass fraction in manifold fluid, with a given inlet flow salt fraction
Sm=zeros(1,chambers+1);
Sm(1)=Sin;

%Temperature of manifold fluid, with a given inlet flow temperature
Tm=zeros(1,chambers+1);
Tm(1)=Tin;

%Temperature distribution in the tank, given
Tt=zeros(1,chambers+2);
Tt(2:chambers+1)=Ttank;

%Salt distribution in the tank, given
St=zeros(1,chambers+2);
St(2:chambers+1)=Stank;

n=2;

%Orifice and wall perforation resistances
%In laminar regime, both orifice and wall perforation resistances a
%function of Re.  Can vary each individual resistance here.
R=[0,Ro,Ro,Ro,Ro,Ro,Ro,Ro,Ro,Ro,Ro,Ro,0];
Rt=[0,2.34e5,3.94e5,2.34e5,Rp,Rp,Rp,Rp,Rp,Rp,Rp,Rp,0];
```

```
%Constants and initialization
g=9.81;

%initialization
Mtsum=0;
Rating=0;


flag1=7;

%Evaluates the pressure in the tank using the salt and temperature
%stratification given.
% P_flip(1)=979.908;
P_flip(1)=0;
T_tflip=fliplr(Tt);
S_tflip=fliplr(St);
for k=2:chambers+1
   P_flip(k)=P_flip(k-1)+rhoC(S_tflip(k),T_tflip(k))*g*z;
end
Pt=fliplr(P_flip);
%   P_t=fliplr(Pt);

finished=chambers+2;

%Equations used to solve for manifold performance
while (n<finished)
    if (Mm(n)>0)
      %Pressure Function
      %Evaluates the manifold pressure at the next node
         Pm(n)=Pm(n-1)-rhoC(Sm(n-1),Tm(n-1))*g*z-(R(n)*Mm(n)^2)/rhoC(Sm(n-
1),Tm(n-1));

        if (Pm(n)>=Pt(n))
          %Evaluates the mass flow through the manifold wall if pressure
          %is greater in manifold than in tank.
          Mt(n)=sqrt(rhoC(Sm(n-1),Tm(n-1))*(Pm(n)-Pt(n))/Rt(n));
          Tm(n)=Tm(n-1);
          Sm(n)=Sm(n-1);
        else
          %Evaluates the mass flow through the manifold wall if pressure
          %in tank is greater than manifold
          Mt(n)=-sqrt(rhoC(St(n),Tt(n))*(Pt(n)-Pm(n))/Rt(n));
          %Mixing in manifold chamber
          Tm(n)=(Mm(n)*Tm(n-1)-Mt(n)*Tt(n+1))/(Mm(n)-Mt(n));
          Sm(n)=(Mm(n)*Sm(n-1)-Mt(n)*St(n+1))/(Mm(n)-Mt(n));
        end
```

```
    Mm(n+1)=Mm(n)-Mt(n); %Evalutes the mass flow at the downstream node
    Mtsum=Mtsum+Mt(n); %Summation of all mass flows out of the manifold.  Should
equal the flow rate at the inlet of the manifold, Min.


      if (Mm(n+1)<0.0002) && (Mm(n+1)>-.0002)
          Mm(n+1)=0;
          flag1=n;
      end


    else

      %If mass flow rate at a node is 0, manifold in equlibrium with tank
      if (n<chambers+2)
      Pm(n)=Pt(n);
      Mt(n)=0;
      Mm(n+1)=0;
      Tm(n)=Tt(n+1);
      Sm(n)=St(n+1);
      end

    end
   n=n+1;

end


%Evaluates the density in the tank and manifold for the purpose of printing
%results
for c=1:chambers+1
Rhom(c)=rhoC(Sm(c),Tm(c));
end
for c=2:chambers+1
Rhot(c)=rhoC(St(c),Tt(c));
end

for t=[2,3]
      %Summation of undesired mass flows exiting or entering the manifold
      Rating=Rating+Mt(t);
end

if (print==1)
    %Prints result of final run
```

```
    Mat=[Mm(1:chambers+1)', Mt', Pm', Pt', Tm', Tt(1:chambers+1)', Sm',
St(1:chambers+1)', Rhom', Rhot']
    Mu=Rating/Mm(2) %Dimensionless undesired flow
    Pr=(Ro*Mm(2)^2)/(9.81*z*Rhom(1)*(Rhot(2)-Rhom(1)))  %Dimensionless
operating condition

end

Mu=Rating/Mm(2); %Dimensionless undesired flow
Pr=(Ro*Mm(2)^2)/(9.81*z*Rhom(1)*(Rhot(2)-Rhom(1)));  %Dimensionless operating
condition
error=Mm(2)-Mtsum; %Should equal 0, as flow entering manifold through inlet should
equal total flow exiting or entering the manifold
end
```

```
%Density (CaCl2)
function y = rhoC(S,T)
	b0 = 1.993771843;   %H2O density function
	b1 = 1.0985211604;
	b2 = -0.5094492996;
	b3 = -1.7619124270;
	b4 = -44.9005480267;
	b5 = -723692.2618632;

	theta = T/647.096;
	tau = 1 - theta;
	rho_crit = 322;      %density of water at critical point kg/m^3
	rho = rho_crit*(1 + b0*tau.^(1/3) + b1*tau.^(2/3) + b2*tau.^(5/3) + b3*tau.^(16/3)
+ b4*tau.^(43/3) + b5*tau.^(110/3));

	r0 = 1.0;          %CaCl2 S_max = 0.60
	r1 = 0.836014;
	r2 = -0.436300;
	r3 = 0.105642;
	psi = S./ (1-S);
	y = rho .* ( r0*psi.^0 + r1*psi.^1 + r2*psi.^2 + r3*psi.^3);
```

```
%Specific heat kJ/kg-k (CaCl2) min 273.15 K
function y = cpC(S,T)
   a0 = 88.7891;
   a1 = -120.1958;
   a2 = -16.9264;
   a3 = 52.4654;
   a4 = 0.10826;
   a5 = 0.46988;

   theta = T/228 - 1;
   cph2o = a0 + a1*theta.^0.02 + a2*theta.^0.04 + a3*theta.^0.06 + a4*theta.^1.8 +
a5*theta.^8;


   A = 1.63799;
   B = -1.69002;
   C = 1.05124;
   D = 0.0;
   E = 0.0;
   F = 58.5225;
   G = -105.6343;
   H = 47.7948;
   f1 = A.*S + B.*S.^2 + C.*S.^3;
   f2 = F.*theta.^0.02 + G.*theta.^0.04 + H.*theta.^0.06;

   y = cph2o .* (1 - f1.*f2);
```

The following is code obtained from MATLAB Central, written by Douglas Schwartz.

```
function [x0,y0,iout,jout] = intersections(x1,y1,x2,y2,robust)
%INTERSECTIONS Intersections of curves.
%   Computes the (x,y) locations where two curves intersect.  The curves
%   can be broken with NaNs or have vertical segments.
%
% Example:
%   [X0,Y0] = intersections(X1,Y1,X2,Y2,ROBUST);
%
% where X1 and Y1 are equal-length vectors of at least two points and
% represent curve 1.  Similarly, X2 and Y2 represent curve 2.
% X0 and Y0 are column vectors containing the points at which the two
% curves intersect.
%
% ROBUST (optional) set to 1 or true means to use a slight variation of the
% algorithm that might return duplicates of some intersection points, and
% then remove those duplicates.  The default is true, but since the
% algorithm is slightly slower you can set it to false if you know that
% your curves don't intersect at any segment boundaries.  Also, the robust
% version properly handles parallel and overlapping segments.
%
% The algorithm can return two additional vectors that indicate which
% segment pairs contain intersections and where they are:
%
%   [X0,Y0,I,J] = intersections(X1,Y1,X2,Y2,ROBUST);
%
% For each element of the vector I, I(k) = (segment number of (X1,Y1)) +
% (how far along this segment the intersection is).  For example, if I(k) =
% 45.25 then the intersection lies a quarter of the way between the line
% segment connecting (X1(45),Y1(45)) and (X1(46),Y1(46)).  Similarly for
% the vector J and the segments in (X2,Y2).
%
% You can also get intersections of a curve with itself.  Simply pass in
% only one curve, i.e.,
%
%   [X0,Y0] = intersections(X1,Y1,ROBUST);
%
% where, as before, ROBUST is optional.

% Version: 1.12, 27 January 2010
% Author:  Douglas M. Schwarz
% Email:   dmschwarz=ieee*org, dmschwarz=urgrad*rochester*edu
% Real_email = regexprep(Email,{'=','*'},{'@','.'})
```

```
% Theory of operation:
%
% Given two line segments, L1 and L2,
%
%   L1 endpoints:  (x1(1),y1(1)) and (x1(2),y1(2))
%   L2 endpoints:  (x2(1),y2(1)) and (x2(2),y2(2))
%
% we can write four equations with four unknowns and then solve them.  The
% four unknowns are t1, t2, x0 and y0, where (x0,y0) is the intersection of
% L1 and L2, t1 is the distance from the starting point of L1 to the
% intersection relative to the length of L1 and t2 is the distance from the
% starting point of L2 to the intersection relative to the length of L2.
%
% So, the four equations are
%
%    (x1(2) - x1(1))*t1 = x0 - x1(1)
%    (x2(2) - x2(1))*t2 = x0 - x2(1)
%    (y1(2) - y1(1))*t1 = y0 - y1(1)
%    (y2(2) - y2(1))*t2 = y0 - y2(1)
%
% Rearranging and writing in matrix form,
%
%  [x1(2)-x1(1)       0       -1   0;      [t1;      [-x1(1);
%       0       x2(2)-x2(1)  -1   0;   *   t2;   =   -x2(1);
%   y1(2)-y1(1)       0        0  -1;       x0;       -y1(1);
%       0       y2(2)-y2(1)   0  -1]       y0]       -y2(1)]
%
% Let's call that A*T = B.  We can solve for T with T = A\B.
%
% Once we have our solution we just have to look at t1 and t2 to determine
% whether L1 and L2 intersect.  If 0 <= t1 < 1 and 0 <= t2 < 1 then the two
% line segments cross and we can include (x0,y0) in the output.
%
% In principle, we have to perform this computation on every pair of line
% segments in the input data.  This can be quite a large number of pairs so
% we will reduce it by doing a simple preliminary check to eliminate line
% segment pairs that could not possibly cross.  The check is to look at the
% smallest enclosing rectangles (with sides parallel to the axes) for each
% line segment pair and see if they overlap.  If they do then we have to
% compute t1 and t2 (via the A\B computation) to see if the line segments
% cross, but if they don't then the line segments cannot cross.  In a
% typical application, this technique will eliminate most of the potential
% line segment pairs.


% Input checks.
```

```
error(nargchk(2,5,nargin))

% Adjustments when fewer than five arguments are supplied.
switch nargin
   case 2
      robust = true;
      x2 = x1;
      y2 = y1;
      self_intersect = true;
   case 3
      robust = x2;
      x2 = x1;
      y2 = y1;
      self_intersect = true;
   case 4
      robust = true;
      self_intersect = false;
   case 5
      self_intersect = false;
end

% x1 and y1 must be vectors with same number of points (at least 2).
if sum(size(x1) > 1) ~= 1 || sum(size(y1) > 1) ~= 1 || ...
      length(x1) ~= length(y1)
   error('X1 and Y1 must be equal-length vectors of at least 2 points.')
end
% x2 and y2 must be vectors with same number of points (at least 2).
if sum(size(x2) > 1) ~= 1 || sum(size(y2) > 1) ~= 1 || ...
      length(x2) ~= length(y2)
   error('X2 and Y2 must be equal-length vectors of at least 2 points.')
end


% Force all inputs to be column vectors.
x1 = x1(:);
y1 = y1(:);
x2 = x2(:);
y2 = y2(:);

% Compute number of line segments in each curve and some differences we'll
% need later.
n1 = length(x1) - 1;
n2 = length(x2) - 1;
xy1 = [x1 y1];
xy2 = [x2 y2];
dxy1 = diff(xy1);
```

```
dxy2 = diff(xy2);

% Determine the combinations of i and j where the rectangle enclosing the
% i'th line segment of curve 1 overlaps with the rectangle enclosing the
% j'th line segment of curve 2.
[i,j] = find(repmat(min(x1(1:end-1),x1(2:end)),1,n2) <= ...
    repmat(max(x2(1:end-1),x2(2:end)).',n1,1) & ...
    repmat(max(x1(1:end-1),x1(2:end)),1,n2) >= ...
    repmat(min(x2(1:end-1),x2(2:end)).',n1,1) & ...
    repmat(min(y1(1:end-1),y1(2:end)),1,n2) <= ...
    repmat(max(y2(1:end-1),y2(2:end)).',n1,1) & ...
    repmat(max(y1(1:end-1),y1(2:end)),1,n2) >= ...
    repmat(min(y2(1:end-1),y2(2:end)).',n1,1));

% Force i and j to be column vectors, even when their length is zero, i.e.,
% we want them to be 0-by-1 instead of 0-by-0.
i = reshape(i,[],1);
j = reshape(j,[],1);

% Find segments pairs which have at least one vertex = NaN and remove them.
% This line is a fast way of finding such segment pairs.  We take
% advantage of the fact that NaNs propagate through calculations, in
% particular subtraction (in the calculation of dxy1 and dxy2, which we
% need anyway) and addition.
% At the same time we can remove redundant combinations of i and j in the
% case of finding intersections of a line with itself.
if self_intersect
    remove = isnan(sum(dxy1(i,:) + dxy2(j,:),2)) | j <= i + 1;
else
    remove = isnan(sum(dxy1(i,:) + dxy2(j,:),2));
end
i(remove) = [];
j(remove) = [];

% Initialize matrices.  We'll put the T's and B's in matrices and use them
% one column at a time.  AA is a 3-D extension of A where we'll use one
% plane at a time.
n = length(i);
T = zeros(4,n);
AA = zeros(4,4,n);
AA([1 2],3,:) = -1;
AA([3 4],4,:) = -1;
AA([1 3],1,:) = dxy1(i,:).';
AA([2 4],2,:) = dxy2(j,:).';
B = -[x1(i) x2(j) y1(i) y2(j)].';
```

```
% Loop through possibilities.  Trap singularity warning and then use
% lastwarn to see if that plane of AA is near singular.  Process any such
% segment pairs to determine if they are colinear (overlap) or merely
% parallel.  That test consists of checking to see if one of the endpoints
% of the curve 2 segment lies on the curve 1 segment.  This is done by
% checking the cross product
%
%   (x1(2),y1(2)) - (x1(1),y1(1)) x (x2(2),y2(2)) - (x1(1),y1(1)).
%
% If this is close to zero then the segments overlap.

% If the robust option is false then we assume no two segment pairs are
% parallel and just go ahead and do the computation.  If A is ever singular
% a warning will appear.  This is faster and obviously you should use it
% only when you know you will never have overlapping or parallel segment
% pairs.

if robust
   overlap = false(n,1);
   warning_state = warning('off','MATLAB:singularMatrix');
   % Use try-catch to guarantee original warning state is restored.
   try
      lastwarn('')
      for k = 1:n
         T(:,k) = AA(:,:,k)\B(:,k);
         [unused,last_warn] = lastwarn;
         lastwarn('')
         if strcmp(last_warn,'MATLAB:singularMatrix')
            % Force in_range(k) to be false.
            T(1,k) = NaN;
            % Determine if these segments overlap or are just parallel.
            overlap(k) = rcond([dxy1(i(k),:);xy2(j(k),:) - xy1(i(k),:)]) < eps;
         end
      end
      warning(warning_state)
   catch err
      warning(warning_state)
      rethrow(err)
   end
   % Find where t1 and t2 are between 0 and 1 and return the corresponding
   % x0 and y0 values.
   in_range = (T(1,:) >= 0 & T(2,:) >= 0 & T(1,:) <= 1 & T(2,:) <= 1).';
   % For overlapping segment pairs the algorithm will return an
   % intersection point that is at the center of the overlapping region.
   if any(overlap)
      ia = i(overlap);
```

```
        ja = j(overlap);
        % set x0 and y0 to middle of overlapping region.
        T(3,overlap) = (max(min(x1(ia),x1(ia+1)),min(x2(ja),x2(ja+1))) + ...
           min(max(x1(ia),x1(ia+1)),max(x2(ja),x2(ja+1)))).'/2;
        T(4,overlap) = (max(min(y1(ia),y1(ia+1)),min(y2(ja),y2(ja+1))) + ...
           min(max(y1(ia),y1(ia+1)),max(y2(ja),y2(ja+1)))).'/2;
        selected = in_range | overlap;
    else
        selected = in_range;
    end
    xy0 = T(3:4,selected).';

    % Remove duplicate intersection points.
    [xy0,index] = unique(xy0,'rows');
    x0 = xy0(:,1);
    y0 = xy0(:,2);

    % Compute how far along each line segment the intersections are.
    if nargout > 2
        sel_index = find(selected);
        sel = sel_index(index);
        iout = i(sel) + T(1,sel).';
        jout = j(sel) + T(2,sel).';
    end
else % non-robust option
    for k = 1:n
        [L,U] = lu(AA(:,:,k));
        T(:,k) = U\(L\B(:,k));
    end

    % Find where t1 and t2 are between 0 and 1 and return the corresponding
    % x0 and y0 values.
    in_range = (T(1,:) >= 0 & T(2,:) >= 0 & T(1,:) < 1 & T(2,:) < 1).';
    x0 = T(3,in_range).';
    y0 = T(4,in_range).';

    % Compute how far along each line segment the intersections are.
    if nargout > 2
        iout = i(in_range) + T(1,in_range).';
        jout = j(in_range) + T(2,in_range).';
    end
end

% Plot the results (useful for debugging).
% plot(x1,y1,x2,y2,x0,y0,'ok');
```